



# Particle Vibration, an Instrument to Study Particle Accumulation Structures On Board the International Space Station

Marcello Lappa<sup>1</sup> · Thomas Burel<sup>1</sup> · Monica Kerr<sup>1</sup> · Georgie Crewdson<sup>1</sup> · Alessio Boaro<sup>1</sup> · Paolo Capobianchi<sup>1</sup> · Sebastien Vincent Bonnieu<sup>2</sup> · Lesley Murphy<sup>3</sup> · Peter Randall<sup>3</sup> · Steven Hens<sup>4</sup>

Received: 1 November 2021 / Accepted: 17 March 2022  
© The Author(s) 2022

## Abstract

The scientific and technological aspects of the PARTICLE VIBRATION Project (also known as T-PAOLA i.e. “Thermovibrationally-driven Particle self-Assembly and Ordering mechanisms in Low gAvity”) are described in detail. The project relies on the combined use of the Selectable Optical Diagnostics Instrument (SODI), a Class-2 device developed by ESA for scientific experiments in the field of fluids on board the International Space Station, and the Microgravity Science Glovebox (MSG), a Class-1 general purpose facility under the responsibility of NASA. The related modular architecture has recently been expanded under the umbrella of new scientific research funded by the UK Space Agency to allow for a novel class of experiments dealing with multiphase (solid-liquid) flows. The final aim of this microgravity project is the identification of new dispersed-phase self-organization phenomena driven by the application of vibrations and the ensuing development of new contactless particle manipulations strategies. In the present paper, emphasis is given to the related space hardware and software, the experiment protocol, the ground tests and procedures and all the adaptations that had to be implemented to overcome a number of technological and physical issues, both general and system-specific.

**Keywords** Microgravity · Facilities · Fluids and Particles · Vibrations

## Introduction

The International Space Station (ISS) provides a unique laboratory in which scientists can observe and study a variety of phenomena that can effectively take place only when weightless conditions are attained, or which would be otherwise hard to study in normal gravity (Lappa 2004; Kitmacher 2010). Relevant exemplars are surface-tension driven (capillary) effects, diffusive transport,

solidification, combustion, boiling and the dynamics of many other multiphase systems (see, e.g., Shevtsova et al. 2011a, b; Mirihanage et al. 2012; Dhir et al. 2012; Triller et al. 2018; Irace et al. 2021). On the surface of our planet, the related mechanisms are often dominated by buoyancy convection (which tends to create pervasive motions in the entire bulk of the considered specimens) or sedimentation (which can force the involved lighter and heavier phases to separate).

By removing the disturbing role played by this force, research conducted in microgravity is supporting current efforts to identify new principles and strategies for the active control of these processes (Lappa 2004). In such a context, of special interest are the dynamics of the so-called *complex fluids*, i.e. media characterized by the coexistence of two phases, namely, a liquid or a gas and a solid (in the form of dispersed fine particles). The special attention paid to these binary mixtures stems from their ability to develop unusual responses enabled by the multiphase nature of the considered medium per se. More precisely, the ensuing macroscopic dynamics are made “complex” by the interrelations or interdependence between macro physical processes

---

✉ Marcello Lappa  
marcello.lappa@strath.ac.uk

<sup>1</sup> Department of Mechanical and Aerospace Engineering, University of Strathclyde, James Weir Building, 75 Montrose Street, Glasgow G1 1XJ, UK

<sup>2</sup> European Space Agency, European Space Research and Technology Centre, Keplerlaan 1, 2201 AZ Noordwijk, Netherlands

<sup>3</sup> Cody Technology Park, QinetiQ, Ively Rd, Farnborough GU14 0LX, UK

<sup>4</sup> QinetiQ Space NV, Hogenakkerhoekstraat 9, 9150 Kruibeke, Belgium

(such as the presence of steady, time-periodic or chaotic bulk convection) and mechanisms taking place on a fine-grained micromechanical level (including, but not limited to, particle collisions and interaction with physical boundaries, viscous and inertial effects at the particle scale and particle networking or caging events).

Multiphase systems of such a kind are omnipresent in technology and microgravity research is currently seeking new ways to advance their exploitation in relation to both terrestrial processes and space technologies. In the former case, relevant applications can be implemented at small length scales where the influence of the gravitational field on fluids is greatly reduced; in the latter, their relevance directly links to the development of future deep space exploration missions for which an improvement in our ability to control fluid phases and/or manufacture materials in situ will play a crucial role.

These concepts apply to both realms of inorganic and organic processes. Almost all structural materials for mechanical and aerospace engineering, many types of composites, plastics, metal and polymer alloys, electrical conductors, and magnetic substances involve the interaction of a dispersed (minority) phase and a fluid matrix (majority phase) at some stage in the manufacturing process (Utracki 1983; Lee and Park 1994; Mason 1999; Prinz and Romero 1993; Ratke 1992; Roths et al. 2002; Lappa 2005; Deng and Chawla 2006). Similarly, many organic materials such as protein crystals or other macromolecular substances, currently being used for the production of drugs and medicines, are obtained in the form of ‘seeds’, which nucleate in a fluid (Carotenuto et al. 2002; Lappa 2011).

Once the effects of gravity are no longer felt, the different densities of the involved phases no longer represent a constraint forcing the dispersed particles to separate from the fluid through sedimentation or flotation; exploring *self-assembly principles* becomes therefore possible. Self-induced particle clustering is indeed emerging as one of the most relevant or promising approaches to develop in-space heterogeneous systems consisting of parts that can recognize and bind to each other or form specific templates or patterns. Relevant exemplars pertaining to this branch of microgravity research are the JEREMI project, i.e. the Japanese European Research Experiments on Marangoni Instabilities (see, e.g., Kuhlmann et al. 2014; Shevtsova et al. 2014a, b) and the PARTICLE VIBRATION project (also known as T-PAOLA i.e. “Thermovibrationally-driven Particle self-Assembly and Ordering mechanisms in Low gravity” experiment, see Lappa and Burel, 2020).

Both concern the possibility to develop new contactless solid-particle manipulation strategies, i.e. to induce phenomena where particles can be naturally driven to occupy certain regions of the physical space without touching them (Lappa 2016a). In particular, the former experiment will target this objective in conjunction with the thermocapillary

(Marangoni) effect in a liquid bridge (a freely floating column of liquid with dispersed solid spherical particles). For the latter, the role of main force driving macroscopic fluid flow will be taken over by thermovibrational effects, namely, convection induced in a non-isothermal cubic enclosure (containing a fluid-particle mixture) *by the application of vibrations with given frequency and amplitude* (the reader interested in this type of convective phenomena may consider, e.g., the recent contributions by Lappa 2016b; Perminov et al. 2021; Boaro and Lappa 2021a, b; Crewdson and Lappa 2021a, b; Lappa and Boaro 2021).

While initial observations of particles demixing from the fluid and forming regular circuits or ‘closed multi-lobe wires’ in oscillatory (supercritical) Marangoni flow dates back to 1996 (Schwabe et al. 1996), the discovery of similar behaviors in thermovibrational flow is much more recent (Lappa 2014a, b). In the latter case, the dynamics are inherently more complex as particle structures manifest in the form of highly regular and multi-dimensional (two-dimensional or three-dimensional) loci of accumulation (see Fig. 1, as opposed to the essentially one-dimensional (filamentary) nature of those typically observed in surface-tension driven flows). Other notable differences concern the underlying mechanisms, which shift from the purely inertial process known to support particle clustering in Marangoni convection (Pushkin et al. 2011; Lappa 2013a, b; Capobianchi and Lappa 2020, 2021a, b) to the more complex and delicate interplay of inertial, thermovibrational and geometrical (container shape) influential factors when the thermovibrational case is considered (Lappa 2014a, b).

A description of the scientific and technological facets of the JEREMI project related to solid particle dynamics in Marangoni flow can be found in Shevtsova et al. (2008). For additional theoretical background relating to the PARTICLE-VIBRATION project, the interested reader may consider Lappa (2016c, 2017, 2019a, b); the present work follows and integrates the information reported in those papers by concentrating on an aspect for which relevant knowledge has not been disseminated yet, that is, a proper description of the purely technological details of this new experiment, namely, an illustration of the challenges associated with exploring the dynamics of vibrated non-isothermal multiphase systems onboard the ISS. Accordingly, most of the available room is used here to discuss critically (i.e. illustrating advantages and bottlenecks) the related space hardware, its utilization, the experiment protocol (main steps) and all the adaptations that had to be implemented to overcome a number of practical issues of various natures. In order to do so, the present paper is organized as follows: In **Space Hardware**, a synthetic account of the experimental hardware is presented. **Experiment Conduct** describes the materials employed and the scientific protocol. **On the ground activities conducted in preparation of the Flight experiment** details the results of the dedicated on-the-ground

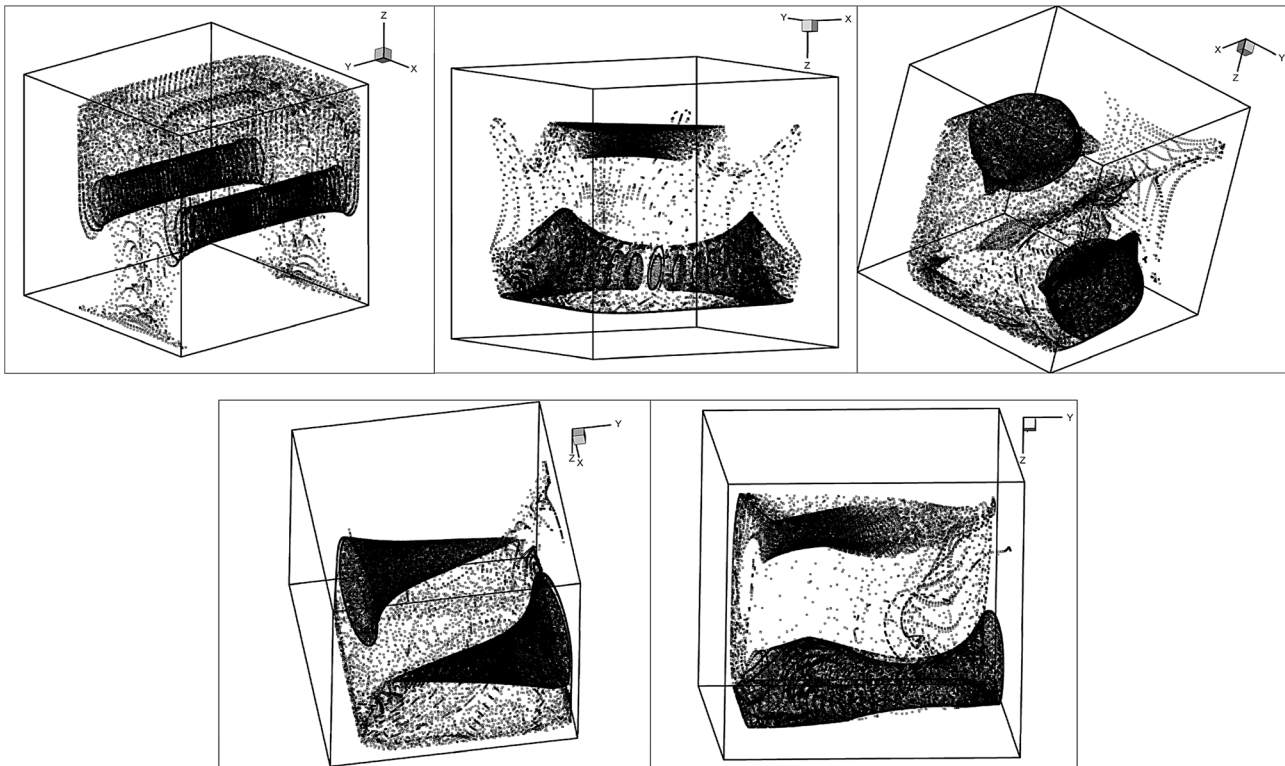


**Fig. 1** Examples of particle structures spontaneously formed by particles in a non-isothermal vibrated dilute liquid-particles system in microgravity (numerical simulations)

activities that have been carried out to reduce risks and optimize some specific aspects of the experiment.

## Space Hardware

In terms of hardware, the PARTICLE VIBRATION experiment heavily relies on the utilization of the so-called Selectable Optical Diagnostics Instrument (SODI). Originally designed to carry out physics experiments in the field of soft matter and fluids for a variety of conditions (Shevtsova et al. 2011a, b; Lappa et al. 2012; Mazzoni et al. 2013; Mialdun et al. 2013, 2018, 2020; Triller et al. 2018; Schraml et al. 2019; Sommermann et al. 2019; Dubert et al. 2020), SODI has been developed by an industrial consortium (led by QinetiQ) in the frame of a dedicated contract with the European Space Agency, and launched to the ISS in 2010. Essentially, it is a payload equipped with various optical diagnostics (which explains its denomination). Moreover, it displays unique properties, which set it apart from ‘companion’ facilities available onboard the ISS such as the Fluid Science Laboratory (FSL) and the Fluid Physics Experimental Facility (FPEF), which also have enjoyed much success over the last ten years. In terms of optical diagnostics, the FSL (hosted in the Columbus

module) allows interferometric observation in two axes by convertible interferometers with active alignment, Digital Holographic interferometry; Wollaston/shearing interferometry; Schlieren mode combined with shearing mode and Electronic Speckle Pattern Interferometry (Albanese et al. 2007, 2010; Trincherro et al. 2008; Futterer et al. 2012; Zaussinger et al. 2020; Born et al. 2021). The FPEF (hosted in the Kibo module) is equipped with CCD and Infrared cameras, a Particle Tracking Velocimetry system for three dimensional velocity field measurement, a Photo-chromic actuator, etc. (Kawamura et al. 2002; Shevtsova et al. 2008). Despite SODI offers less capabilities, it presents some notable distinguishing marks (as further detailed in the following subsections), which explain why it has been preferred to these larger-scale facilities in many circumstances.

Although the lack of direct data and power interfaces to the main corresponding interfaces of the ISS might be regarded as a limitation, this is the main reason for which its design is very compact. Moreover, it is based on a highly modular architecture, which should be regarded as a great advantage; unlike FSL and the FPEF, which house inside the rack all the subsystems listed above (the commutation from one diagnostic to the other being achieved by inserting specific elements in the optical path), SODI consists of several subsystems which are installed or not depending on the category of phenomena under investigation.

## SODI Basic Inserts and the MSG

In such a context, the PARTICLE VIBRATION experiment has been designed to take full advantage of the SODI specific design and modular concept by maximizing the versatility of the experiment while minimizing the investments required for the development and launch of the needed hardware (the cost for the development of such hardware being only a fraction of that required for an equivalent experiment container to be used in conjunction with other facilities such as the aforementioned FSL).

The main objective of the this section and the next one is therefore a presentation of the modules of SODI required for the execution of the PARTICLE VIBRATION experiment, namely, the very general ones (common to all experiments, described in the present section) and those expressly required to contain, shake and visualize the fluid-particle mixtures at the basis of PARTICLE VIBRATION (**PARTICLE VIBRATION specific hardware**). The former can be introduced as follows:

The Facility Control Unit (FCU, see Fig. 2a) includes the drivers that control all SODI functions, i.e. the drivers for the laser diodes, the measurement from temperature sensors, the USB\_2 to SPI\_2 interface module, the digital and analog interfaces, the Peltier / Heater drivers and the (PIM2403) drivers for translation mechanisms. Importantly, it also hosts the Accelnet Micro Panel (AMP) motor driver of the vibration mechanism specifically needed for the PARTICLE VIBRATION experiment (see **PARTICLE VIBRATION specific hardware**).

The Image Processing Unit (IPU) is another required vital sub-system (Fig. 2b). It consists of a single-board computer and a set of exchangeable hard drives for the storage of images and other data.

Being a Class-2 payload, i.e. a specific kind of hardware that cannot be used in a stand-alone configuration on the ISS (given the lack of direct data and power interfaces to the main corresponding interfaces of the ISS), SODI partially relies on the potentialities offered by the Microgravity Science Glovebox (MSG). In turn, MSG is a Class-1 facility

(fitting the International Standard Payload Rack interfaces of the ISS, Hashimoto et al. 1998) developed by the European Space Agency (ESA) and integrated by NASA Marshall Space Flight Center (MSFC), see Fig. 3.

The different ‘basic’ inserts of the SODI hardware must be installed inside the Work Volume (WV) of MSG in order to be fed with the required power, exchange data with ground and satisfy the necessary level of containment (as we will see in **Materials (Fluids and particles)** when some potentially hazardous liquids are involved in the experiments, 3 distinct levels of confinement are needed, one of which is provided by the MSG WV itself).

Communication between the IPU and the MSG is implemented via a serial data link, which allows ground control. Moreover, an Ethernet link between the IPU and the MSG laptop computer also allows science data transfer for intermediate analysis by on-the-ground science teams. The IPU is powered through the main (120 V) and secondary (28 V) lines provided by the MSG, which are able to feed SODI with the 230 W required during operations.

### Particle Vibration Specific Hardware

For PARTICLE VIBRATION some additional ‘experiment specific’ hardware has been developed.

The related experimental setup consists of small cubic cells, each filled with a different fluid–solid particle mixture (the reader being referred to **Experiment Conduct** for additional details about these mixtures).

Each cell (Fig. 4a) is equipped with Peltier elements (TM-71–1.4–3.7) controlled by the FCU in order to establish the desired temperature difference across the fluid (needed to generate thermovibrational convection in the presence of vibrations). The relative position of the Peltier elements with respect to the direction of vibrations and the fluid cell is shown in Fig. 4b (the temperature gradient is perpendicular to the shaking direction). Moreover, each cell has ‘two’ windows allowing visualization of particles along two perpendicular directions. This is depicted in Fig. 4c, where the related mirrors have also been sketched (both planes yz and

**Fig. 2** SODI basic elements: (a) Facility Control Unit (FCU); (b) Image Processing Unit (IPU)

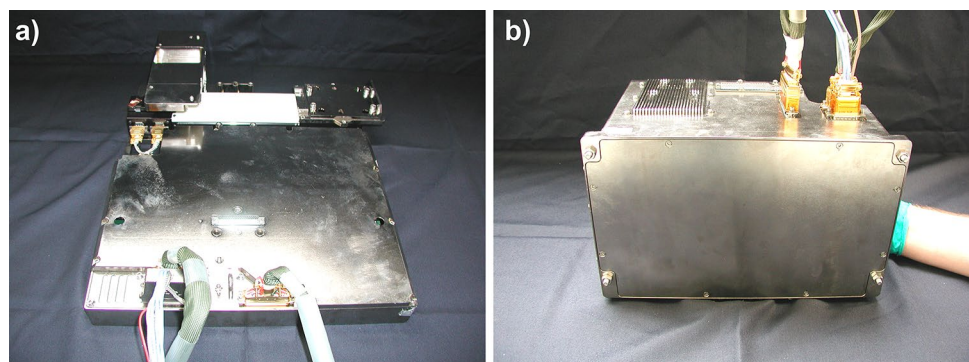
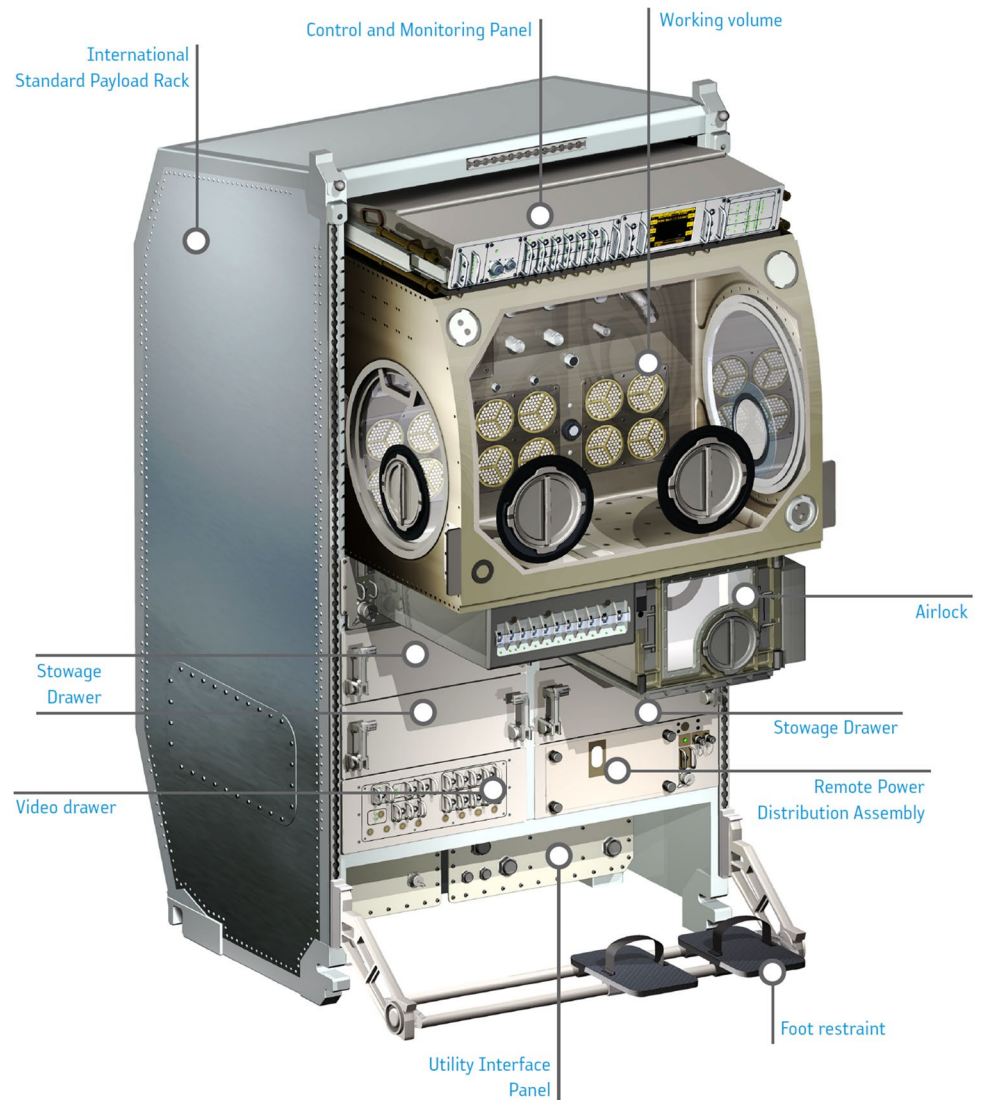


**Fig. 3** MSG isometric view (courtesy of NASA)



xz can be visualized at the same time). Additional details are provided in Fig. 5.

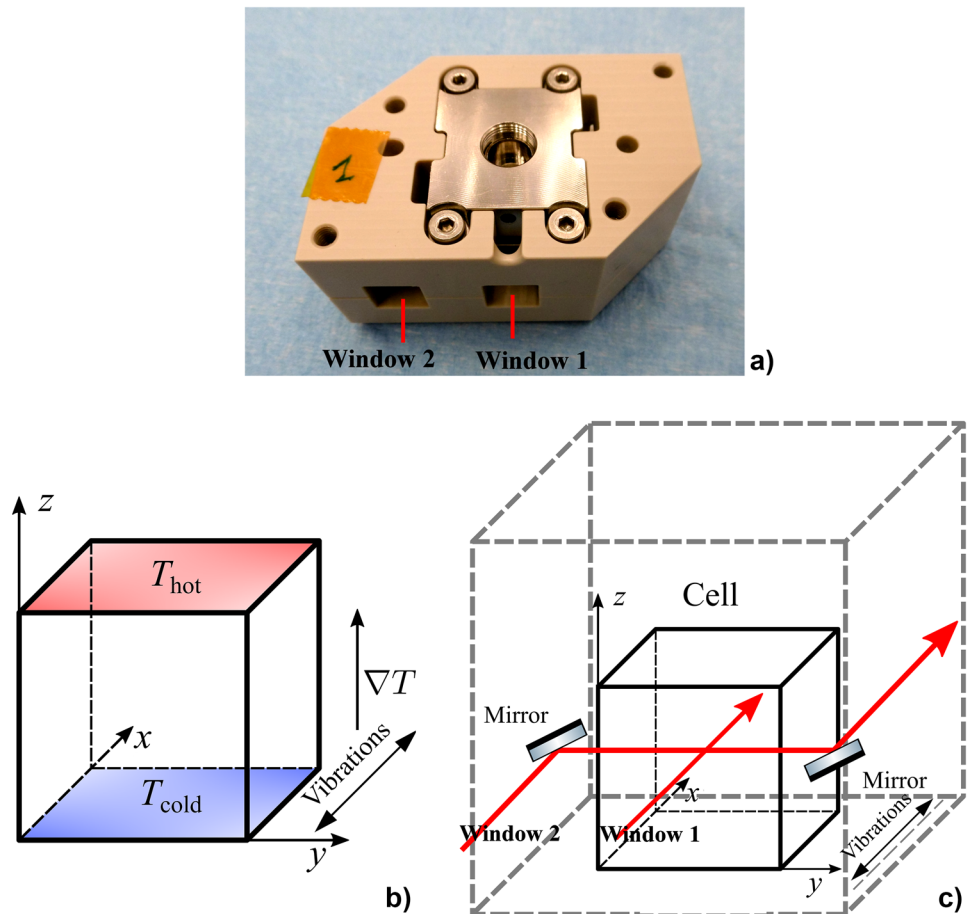
The geometrical size of the experiment volume is  $10 \times 10 \times 10 \text{ mm}^3$ , with aspect ratio (thermal path length/optical path length) of 1.0. Each cell is also equipped with two thermistors, a thermostat (to ensure protection against over-heating), a thermal expansion compensation system and a filling system.

The glass cell is 14 mm thick with a  $10 \times 10 \text{ mm}^2$  cut out inside for the experiment liquid. The cut out is closed at both ends with 2 mm protruding end caps in Nickel-plated copper. Two Viton seals between each end cap and the quartz cube are installed to achieve 2 levels of containment. Additionally a Titanium spacer is added between the copper end caps to prevent the primary load path to go through the glass. The Titanium material is selected for these spacers because of its high stiffness which minimize the creep effect due to compression load and it has a low thermal conductivity to reduce

the heat transfer from the hot side to the cold side of the cell. To increase the thermal resistance between the two sides of the cell, a PEEK bushing is also used to insulate the cell bolts to the Copper and spacers. The whole cell is surrounded by PEEK to improve the thermal insulation. In order to minimize the heat transfer from one end-cap to another, PEEK spacers are inserted between the screws and the end-cap.

The thermal expansion compensation system consists of a sheet (Kalrez) that is located in front of a volume corresponding to the maximum expansion volume that can occur. As a result of a pressure change due to a temperature change inside the cell volume, the sheet will deform allowing a volume change and maintaining the pressure inside the observation volume at a quasi-constant value. The nut fixing the Kalrez sheet in its nominal position has other two O-rings on its outer diameter to guarantee 2 levels of containment. If the nut becomes loose, it is still contained within the cell due to the peltier element covering the copper blocks.

**Fig. 4** Picture (a) showing the fluid cell and the related windows, (b) reference coordinate system of the fluid cell, (c) possible light paths in the fluid cell



Such cells are not operated separately, rather, they are hosted in groups of two inside SODI specific “cell arrays” (see Fig. 6).

The PARTICLE VIBRATION cell arrays have been developed on the basis of the design used for the earlier IVIDIL experiment, however, completely new elastomers and thermostats have been selected to make the hardware compatible with the liquid used for the new experiments and the related specifications.

The main functions of the cell arrays can therefore be summarized as follows:

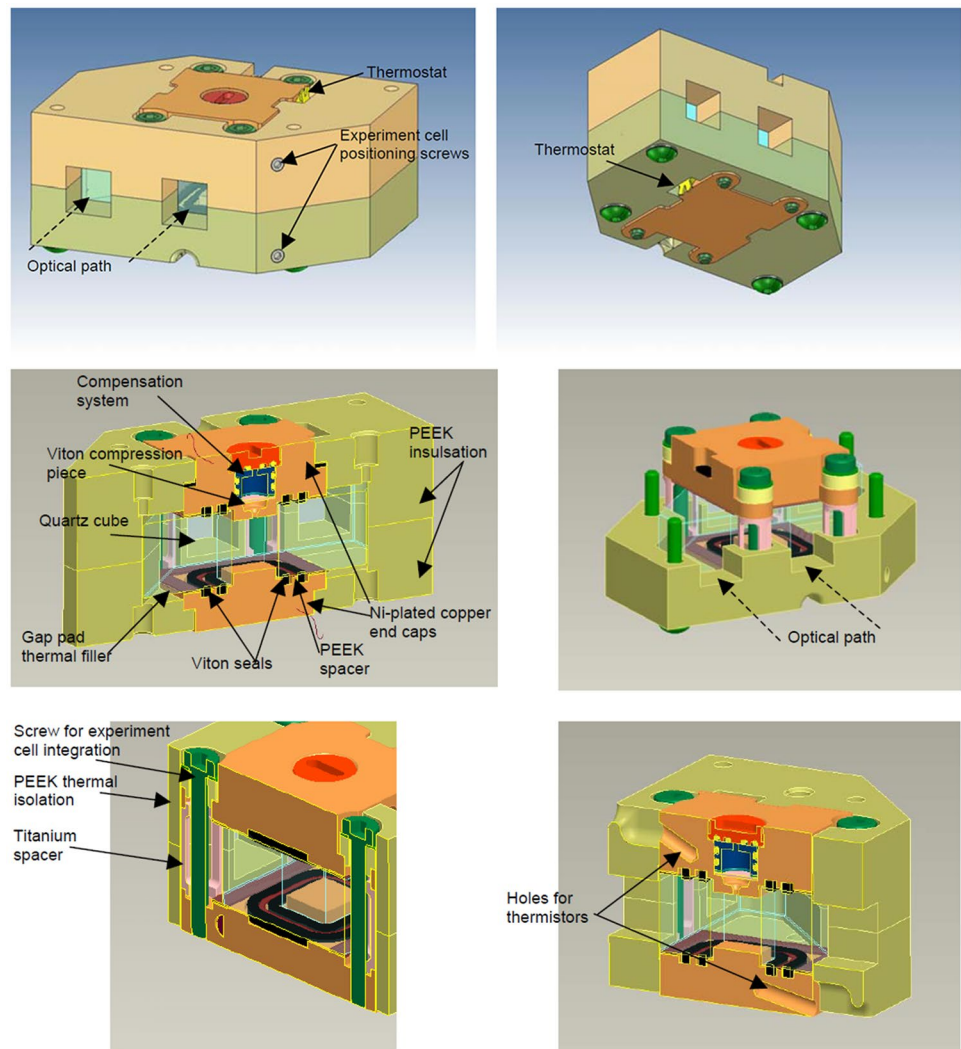
- Guarantee a two-level confinement of the liquids.
- Contain two sample cubic containers (cells), allow for their replacement within the SODI facility and keep them aligned with the optical modules;
- Provide thermal control to the sample cells during the experiment;

Since, as explained above, the experiment requires direct visualization of the particles dispersed in a transparent fluid, optical components also contribute to the final instrument setup. These are the so-called Fixed and Moving Optical Modules shown in Figs. 7a and b, respectively.

This specific denomination originates from the possibility to change the position of one of the two modules along the  $y$  axis (refer to Fig. 6), whereas the other module occupies a fixed position. Since in the PARTICLE VIBRATION experiment there is no need to reposition the moving module, in practice, both can be considered located at permanent positions. They essentially align with the fluid containers hosted in each cell array as indicated in Fig. 8a. In particular, the experiments in these containers (hereafter simply referred to as “primary cell” and “companion cell”) take place in parallel to save microgravity time (i.e. both cells are active at the same time during nominal experiment execution activities). As sketched in Fig. 8a, the Moving Optical Module is used to perform the optical observation of cell 1, while the Fixed Optical Module observes cell 2.

In particular, for PARTICLE VIBRATION, particle visualization entirely relies on a red laser 670 nm (Hitachi 6714G) (see Fig. 8b for a schematization of the Mach-Zehnder interferometer). Finally, the optical systems (both fixed and moving) are equipped with a CCD camera Pantera SA 2M30 (manufactured by Dalsa) with a resolution of  $1920 \times 1080$  (the maximum frame rate, around 15 fps,

**Fig. 5** PARTICLE VIBRATION cell details



is limited by the overall data acquisition system, including the ethernet link; in practice, however, PARTICLE VIBRATION requires only a very low frame rate, with a maximum of 0.56 fps and typically much lower).

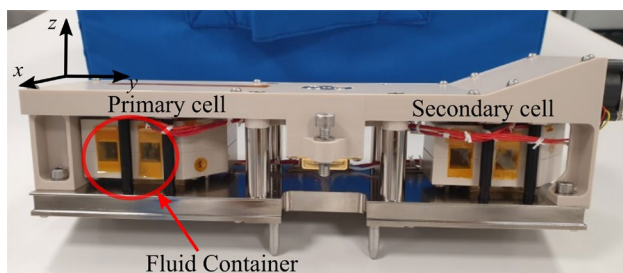


**Fig. 6** PARTICLE VIBRATION cell array, composed of a primary and a secondary cell. Each cell array hosts two fluid containers. Four distinct windows can be seen because each fluid container has two windows (allowing visualization of particles along two perpendicular directions)

An additional component is used to shake the cell array, i.e. to generate vibrations (the other necessary ‘ingredient’ to produce thermovibrational convection). This subsystem (Fig. 9, official nomenclature “IVIDIL Vibration Mechanism”, hereafter, for brevity, simply referred to as the ‘shaker’) creates a sinusoidal displacement of the cell array along the x direction and can be set to various frequencies and amplitudes. It has been designed to align the moving optical module with the experiment cells and must be mounted on the SODI bottom plate as illustrated in Fig. 10.

A simple mathematical expression accounting for the sinusoidal displacement of the cell array along the x axis with respect to a fixed reference frame (e.g., the MSG WV) can be cast in compact form as:

$$\underline{s}^{\text{lab}}(t) = b\sin(\omega t)\hat{u} \tag{1}$$

**Fig. 7** Fixed (a) and Moving (b) Optical Modules

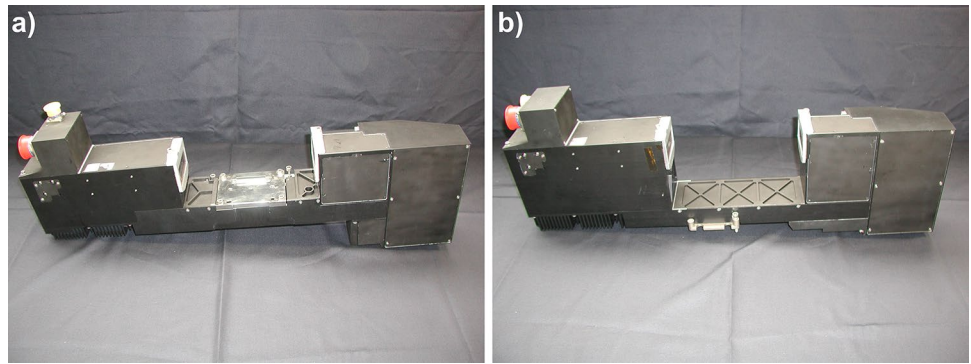


**Fig. 8** (a) Relative position of the optical modules and the fluid containers inside the cell array, (b) light path in the optical system

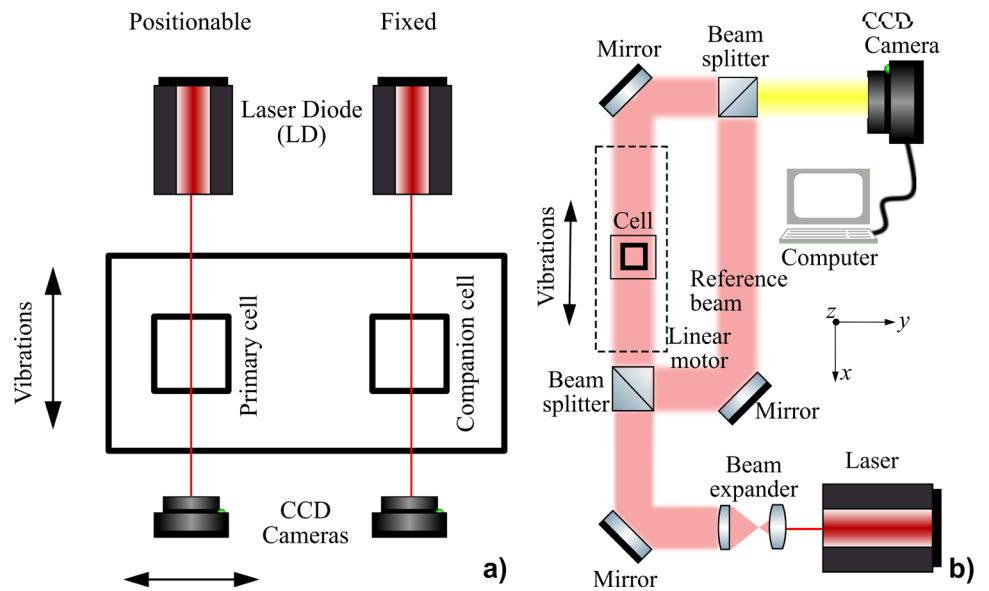


**Fig. 9** The shaker

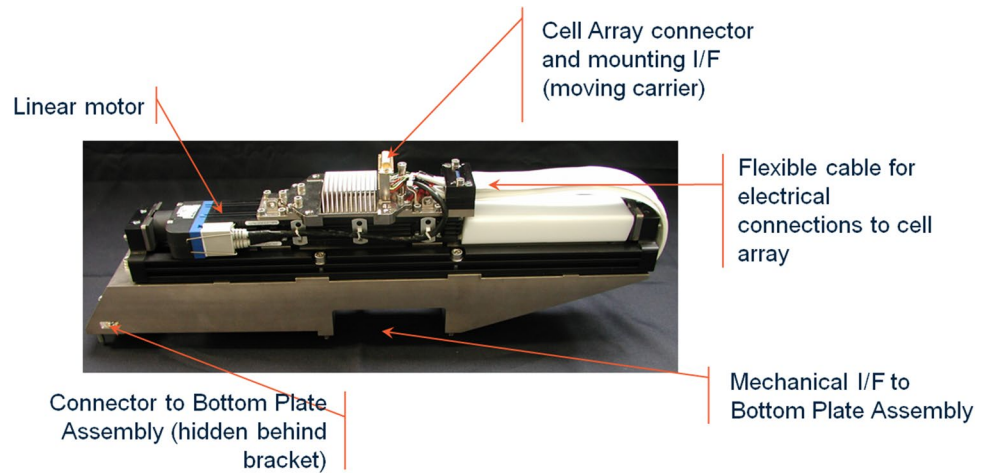
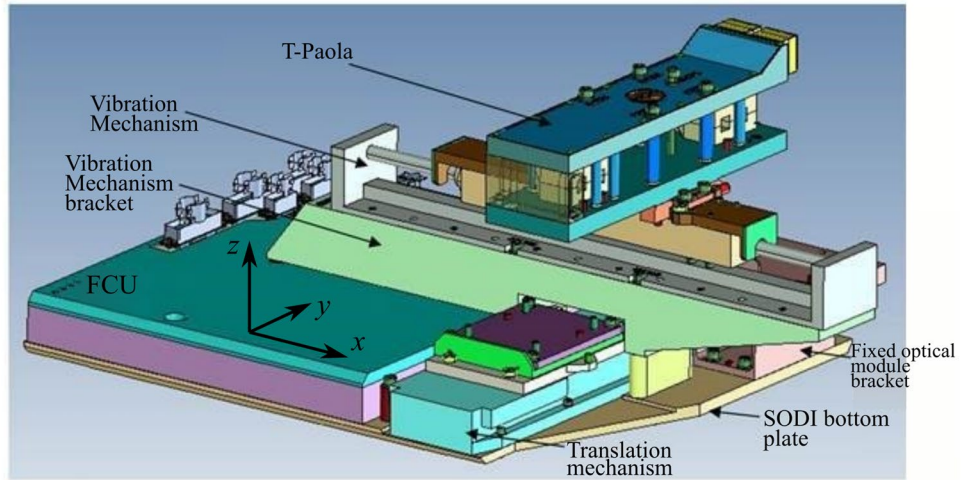


**Fig. 10** The SODI translation mechanism (sketch)



where  $b$  is the amplitude,  $\omega = 2\pi f$  is the angular frequency of the displacement and  $\hat{n}$  is the unit vector along the direction of vibrations. The ensuing time-varying acceleration can be derived mathematically by taking the second derivative of Eq. (1) with respect to time, i.e.

$$\underline{g}(t) = g_\omega \sin(\omega t) \hat{n} \text{ where } g_\omega = b\omega^2 \tag{2}$$

which indicates that the relationship between the amplitude of the acceleration and the vibration frequency is quadratic (namely  $g_\omega$  given by the product of the vibrations amplitude and the square of their angular frequency, see Fig. 11).

Notably, Eq. (2) satisfies the following condition (Eq. (3)):

$$\begin{aligned} \frac{\omega}{2\pi} \int_0^{2\pi/\omega} \underline{g}(t) dt &= \frac{\omega}{2\pi} g_\omega \hat{n} \int_0^{2\pi/\omega} \sin(\omega t) dt \\ &= -\frac{1}{2\pi} g_\omega \hat{n} [\cos(\omega t)]_0^{2\pi/\omega} = 0 \end{aligned} \tag{3}$$

i.e. its time-averaged value over one period of oscillation  $2\pi/\omega$  is exactly zero.

Although, from a purely theoretical standpoint, the shaker is capable of operating at a broad range of frequency/amplitude combinations (as shown in Fig. 11), limited only by the amount of power the electronic driver can deliver to drive these accelerations, for SODI, a discrete number of combinations (known as ‘modes’) were selected and tested by ESA as to avoid exceeding  $\mu\text{g}$  disturbances. Therefore,

**Fig. 11** Relation between vibration amplitude  $b$  and frequency ( $f = \omega/2\pi$ ) and acceleration ( $b\omega^2$ ) reported as a fraction of the equivalent terrestrial acceleration  $9.81 \text{ m/s}^2$

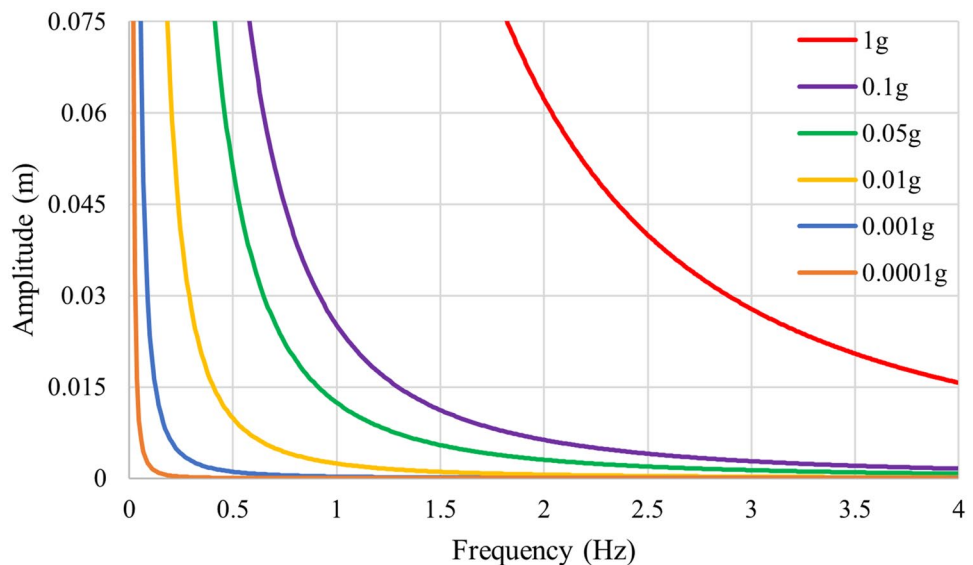


**Table 1** Allowed frequencies and amplitudes (not to exceed the ISS requirements):  $\omega$  and  $b$  are the vibration frequency and amplitude, respectively and  $g_0$  is the standard gravitational acceleration

Mode	Frequency $f$ (Hz)	Amplitude $b$ (m)	Acceleration $b\omega^2$ (m/s <sup>2</sup> )	$b\omega^2/g_0$
1	0.05	$7 \times 10^{-2}$	$7 \times 10^{-3}$	$7.1 \times 10^{-4}$
2	0.1	$7 \times 10^{-2}$	$2.7 \times 10^{-2}$	$2.75 \times 10^{-3}$
3	0.2	$7 \times 10^{-2}$	0.11	$1.1 \times 10^{-2}$
4	0.5	$7 \times 10^{-2}$	0.7	$7.1 \times 10^{-2}$
5	1	$5 \times 10^{-2}$	2	0.2
6	1	$7 \times 10^{-2}$	2.8	0.285
7	2	$2.5 \times 10^{-2}$	3.9	0.4
8	2	$3.1 \times 10^{-2}$	4.9	0.5
9	2	$6.2 \times 10^{-2}$	9.8	1
10	2.8	$2.0 \times 10^{-2}$	6.2	0.6
11	2.8	$2.5 \times 10^{-2}$	7.7	0.9
12	2.8	$3.1 \times 10^{-2}$	9.6	1

the modes reported in Table 1, represent the combinations of vibrations amplitude and frequency that can be effectively implemented on board the ISS for the PARTICLE VIBRATION experiment.

The shaker was previously used for the so-called IVI-DIL experiment (Shevtsova et al. 2011a, b). It was downloaded from ISS in December 2019 and refurbished in order to accommodate the PARTICLE VIBRATION experiment.

## PARTICLE VIBRATION Payload Functional Overview

### On Orbit Assembly

As illustrated in detail in the preceding section, the different modules, which together form the SODI facility, are separate units; this implicitly requires that the crew has to assemble them in orbit. In order to allow for an easy assembly, all units have been designed in such a way that they allow an easy mechanical and electrical integration:

- Mechanical interface: each of the modules is equipped with alignment pins guaranteeing the tolerance needed for proper functioning of the complete SODI facility after removal, maintenance and replacement of a module.

- Electrical interface: connectors are included on each module.

More precisely, all the hardware, except from the IPU E-box (electronic box), has to be installed on the bottom plate, which is mounted in the cold plate of the MSG WV. After the MSG has been configured, the installation of SODI inside the MSG is a common task generally requiring one crew member only. The procedure, consisting of the installation of the bottom plate, the IPU, the optical modules, the

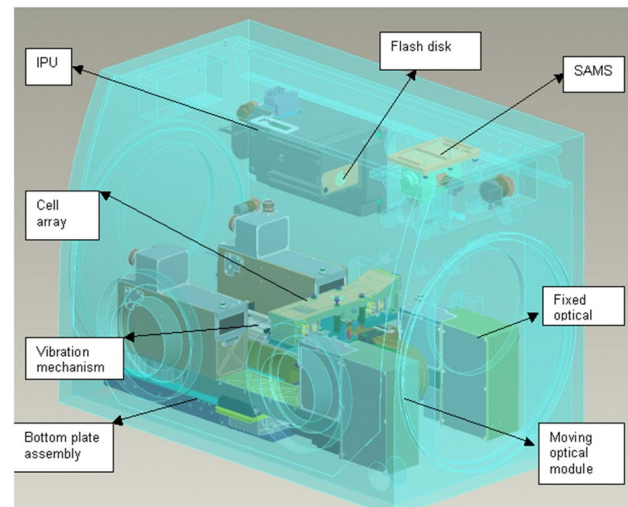


**Fig. 12** Sketch of the MSG WV with all SODI components inside (including the PARTICLE VIBRATION cell array)

shaker and the cell array (Figs. 12 and 13) is estimated to take a time between 2 and 3h.

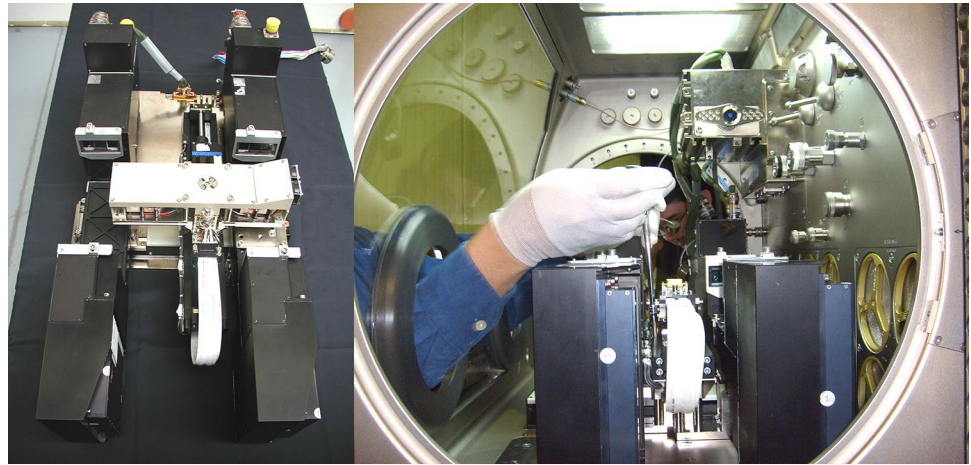
Remarkable crew time savings (whose availability remains scarce despite the efforts by the major national and international agencies to increase the number of astronauts on board the ISS) are also made possible by another fundamental property of this payload, that is the ability of the instrument to execute the experiments on the basis of a ‘script’ (i.e. a sequence of instructions coded in a specific programming language) loaded in the memory of the IPU. Among other things, this modus operandi also allows ground operators (monitoring the instrument 24 h / 7 days) to stop or modify the sequence of experiments by uploading a new script from ground.

### Software and Scripts

The SODI file system relies on of two physical devices: the fixed internal FDD (Flash Disk Drive) with operating system, SODI ASW (Application Software) and timeline script files and the removable Hard disk for storing runtime data (image files and telemetry recording). Upon applying power to the instrument, it:

- Automatically starts the SODI Application Software, which, in turn:
    - Starts the transmission of status data (to ground).
    - Detects the hardware ID tag of the cell array installed.
- Given this basic scenario, the SODI ASW accepts ground commands to:
- Manipulate the timeline state.
  - Manipulate files on the SODI file-system.
  - Exchange files with the SODI external interfaces.

**Fig. 13** Final configuration of the SODI hardware including the FCU, the IPU, the shaker, the optical modules and the cell array



- Manipulate individual actuators in the system (off-nominal operations).

The “Experiment timeline scripts” represent the core (in terms of software) of the experiments and have been developed according to the specific requirements of the PARTICLE VIBRATION project. In the basic configuration, SODI scripts are started via ground command: the experiment is started and executed according to an execution table. The execution table of the experiment describes all the needed actions. It contains information such as temperature set points, duration of each step, image acquisition rate, configuration of the optical diagnostics (laser diodes, shutters, mirrors), activation of the shaker or thermo-modulation process (related details being provided in [Experiment Protocol](#)).

## Experiment Conduct

### Experiment Governing Parameters

As explained to a certain extent in the introduction, the particle accumulation phenomena considered by the PARTICLE VIBRATION project are driven by the delicate interplay *between inertial and thermovibrational effects* (Lappa 2014a, b, 2016c, 2017, 2019a, b; Lappa and Burel 2020). While the former can be put in direct relation with the relative density of particles with respect to the surrounding liquid, their diameter and the acceleration induced by vibrations, the latter depend on the thermal and viscous properties of the considered liquid, the vibration frequency and the imposed temperature difference ( $\Delta T$ ). In other words, this means that the considered problem *depends on six independent influential factors or parameters*: (1) vibration frequency ( $\omega$ ); (2) vibration amplitude ( $b$ ); (3) temperature difference ( $\Delta T$ ); (4) viscosity and thermal

diffusivity of the considered liquid ( $\nu$  and  $\alpha$ , respectively); (5) particle-to-fluid density ratio ( $\xi$ ); (6) particle radius ( $R_p$ ).

The first three parameters can be changed using the specific hardware considered for the experiments (described in [Space Hardware](#)), the other three physical variables depend on liquids and particles.

The non-dimensional groups that depend only on the hardware (i.e. can be varied by changing specific settings of the hardware) can be expressed in non-dimensional form as:

$$\Omega = \frac{\omega L^2}{\alpha}; \gamma = \frac{b\omega^2 L^3}{\alpha^2} \text{ and } Ra_\omega = \frac{b\omega^2 \beta_T \Delta T L^3}{\nu \alpha} \quad (4)$$

where  $\Omega$  is the non-dimensional angular frequency of vibrations,  $\gamma$  is the non-dimensional amplitude of the resulting acceleration and  $Ra_\omega$  is the well-known Rayleigh number ( $\beta_T$  and  $\Delta T$  being the fluid thermal expansion coefficient and the imposed temperature difference, respectively) and  $L$  is the size of the fluid container. The kinematic viscosity and the thermal diffusivity of the considered liquid can be combined into a single non-dimensional parameter, i.e. the Prandtl number (Pr). Besides Pr, the second set of three parameters (those not depending on the hardware) also includes the aforementioned particle-to-fluid density ratio and the so-called particle Stokes number (sixth influential parameter) defined as:

$$St = \frac{2 R_p^2}{9 L^2} \quad (5)$$

The PARTICLE VIBRATION experiments may be regarded as a parametric investigation where the spatial extension, formation time and morphological properties of the highly-ordered particle structures emerging in the considered fluid-particle mixtures are studied as a function of a subset of the influential factors illustrated above (see again Eqs. (4) and (5)). In particular, Table 2 summarizes the influential

**Table 2** Parameters considered for the experiments

Influential factors	Baseline
Vibration frequency ( $\omega$ )	Included (different vibrational modes considered)
Vibration amplitude (b)	Included (different vibrational modes considered)
Temperature difference ( $\Delta T$ )	Included (ranging from 0.5 °C to the maximum possible value allowed by the hardware and the maximum volume expansion)
Type of liquid (Pr)	Not included (single liquid considered)
Particle-to-fluid density ratio ( $\xi$ )	Included (different density ratios considered)
Particle radius ( $R_p$ )	Included (particle with different diameters considered)

factors that are changed or kept constant. While all the PARTICLE VIBRATION experiments are based on a single liquid, four different types of particles are considered (differing with respect to density and/or diameter, see [Materials \(Fluids and particles\)](#)).

Thereby, the following is allowed in terms of scientific outcomes:

- Analysis of the influence of the imposed temperature difference ( $R_{a_0}$ ) on particle structure spatial extension and formation time;
- Analysis of the progression from symmetric to asymmetric particle structures when the Rayleigh number is increased;
- Assessment of the role played by the frequency of vibrations ( $\Omega$ );
- Study of the relationship between particle structure spatial extension (and formation time) and the amplitude of the acceleration ( $\gamma$ );
- Study of the relationship between particle structure spatial extension and formation time and particle-to-fluid density ratio;
- Analysis of the influence of particle diameter on such dynamics.

## Materials (Fluids and Particles)

The materials selected for the space experiments are illustrated in Tables 3, 4 and 5.

Ethanol is a potentially hazardous substance for the crew, therefore requiring a three-level confinement (two levels surrounding the cell array and one level surrounding the work volume in which the entire cell array is installed together with the other SODI components). Tween 20 is a non-ionic surfactant with limited hazardous properties, able to prevent particles staying on surfaces due to electrostatic effects. Under a thermal gradient, a non-ionic substance is preferable to limit the binary diffusion which could induce a spurious flow in the fluid-particle mixture. However, this substance may not be stable at temperature above 40 °C and it would be solid under 0 °C, which should be regarded as general constraints for the entire project.

The compatibility of the materials with the SODI hardware, reported in Tables 3, 4 and 5, has been verified in the framework of long duration compatibility tests conducted by the Payload Developer (i.e. QinetiQ, these tests are described in [Compatibility tests](#)). The ability of particles to resist (without showing damage) the typical spectrum of accelerations produced during the launch has also been assessed ([Vibration Test](#)).

**Table 3** Fluid properties

Fluid	Ethanol Absolute $\geq 99.8\%$	Tween20
Product Number	20821.296	0777-1L
Product dealer	VWR	VWR
Product manufacturer	VWR	VWR
CAS number	64-17-5	9005-64-5
Viscosity [cSt]	1.36 (25 °C)	
Density [kg/m <sup>3</sup> ]	789 (25 °C)	1100 (20 °C)
Volumetric thermal expansion coefficient [1/K]	$1.26 \times 10^{-3}$ (25 °C)	
Freezing point [°C]	-117	
Boiling point [°C]	78	> 100
Heat capacity [J/(kg K)]	2840 (25 °C)	
Thermal conductivity [W/(m K)]	0.169 (25 °C)	

**Table 4** Surfactant

Commercial name	CAS number	Cloud Point (°C)	Surfactant type
Tween 20	9005-64-5 (VWR)	95	Non-ionic

Before starting to deal with these aspects, the next section (Experiment Protocol) includes a complete description of the experiment protocol in terms of thermal boundary conditions, stages of evolution and related temporal sequence.

### Experiment Protocol

For each cell array (Table 6), the experiment protocol consists of a set of ‘runs’ differing in the magnitude of the imposed temperature difference and in the frequency and amplitude of the applied vibrations (as shown in Lappa 2014a, b, 2016c, 2017, 2019a, b; Lappa and Burel 2020, for a fixed value of  $Ra_\omega$ , the geometrical properties of the emerging particle structures depend on the vibration frequency  $\omega$  and exploration of this dependence is the ‘core’ task of the PARTICLE VIBRATION project).

The experimental procedure is structured in 5 steps for each run, as follows:

- **Step 1:** A constant and uniform temperature is established inside the fluid by means of “active” peltier control:  $T$  is set equal to  $T_{avg} = 22\text{ °C}$  i.e. the average temperature inside the MSG (this is needed to reduce heat loss effects).
- **Step 2:** A temperature difference is applied across the sample. The temperature gradient is implemented by

increasing and decreasing the temperature on the two opposite sides of the fluid container in a symmetric way (with respect to the abovementioned fixed reference temperature  $T_{avg}$ ). The temperature difference is maintained for a time sufficiently long to establish a perfect thermally diffusive (linear) temperature profile inside the liquid (no vibrations are applied in this stage; related numerical simulations conducted using ANSYS Fluent can be seen in Fig. 14).

- **Step 3:** The shaker is switched on at a desired frequency and amplitude while keeping the imposed temperatures on the (top and bottom) walls *constant*. In this stage particle structures are formed (the duration of this stage depends on the considered particle radius and density and vibration frequency, ranging from a few hours to one or more days, Fig. 15).
- **Step 4:** A new frequency and a new amplitude of vibrations are set to force the particles to re-disperse in the fluid in preparation of the next experiment. In this stage the temperature on the walls is not kept constant, rather it is sinusoidally changed in time (Fig. 16).

Moreover, a phase shift ( $\Delta\varphi = \pi/2$ ) is intentionally established between the two opposite walls, that is:

$$T_{left} = T_{avg} + \frac{\Delta T_{mod}}{2} \sin(\omega_{therm}t) \tag{6}$$

$$\begin{aligned} T_{right} &= T_{avg} + \frac{\Delta T_{mod}}{2} \sin(\omega_{therm}t + \pi/2) \\ &= T_{avg} + \frac{\Delta T_{mod}}{2} \cos(\omega_{therm}t) \end{aligned} \tag{7}$$

**Table 5** Particles

Array	Particle type	Density (g/cm <sup>3</sup> ) (Density ratio)	Particle Diameter (µm)	Particle material	Supplier
1	Light	0.14 (0.18)	75–90	Silver Coated Hollow Glass	MTL (Microsphere Technology Ltd.)
1	Extra Heavy	2.76 (3.50)	75–90	Silver Coated (Solid Glass with 4% silver)	Hart Material + MLT
2	Heavy & Small	2.24 (2.84)	53–63	Silver Coated Borosilicate Solid Glass	MLT
2	Heavy	1.32 (1.65)	75–90	Silver Coated Hollow Glass	MLT

**Table 6** Array and cell composition

	Cell Array 1		Cell Array 2	
	Primary cell	Companion cell	Primary cell	Companion cell
Liquid	Ethanol	Ethanol	Ethanol	Ethanol
Particles	Light particles	Extra Heavy particles	Small Heavy particles	Heavy particles

**Fig. 14** (a) Technical drawing of the PARTICLE VIBRATION fluid cell (the yellow, white and blue colors are used to indicate solid copper, the quartz thick walls and the fluid domain with the related filling port, respectively); (b) Computational mesh; (c) Temperature distribution established in the fluid and quartz regions in microgravity conditions. The temperature distribution in the quartz region indicates that it can adequately be represented as a linear distribution (purely ‘conducting wall’ behavior)

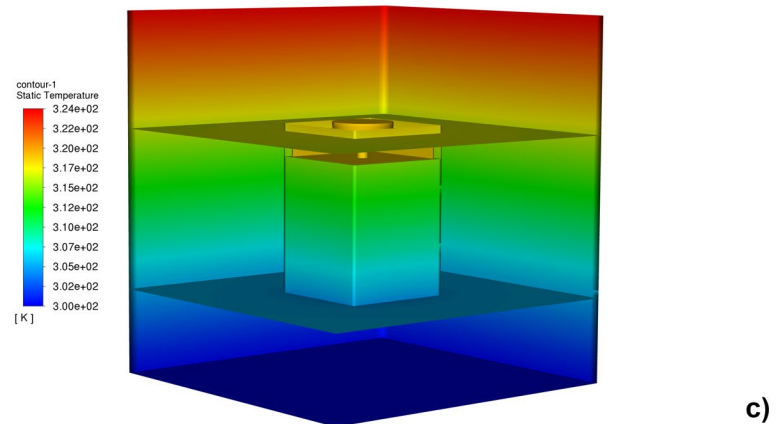
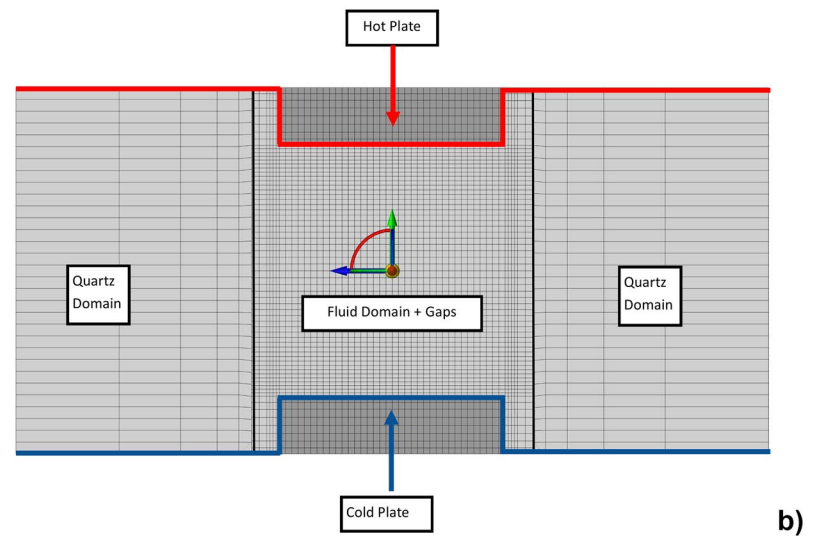
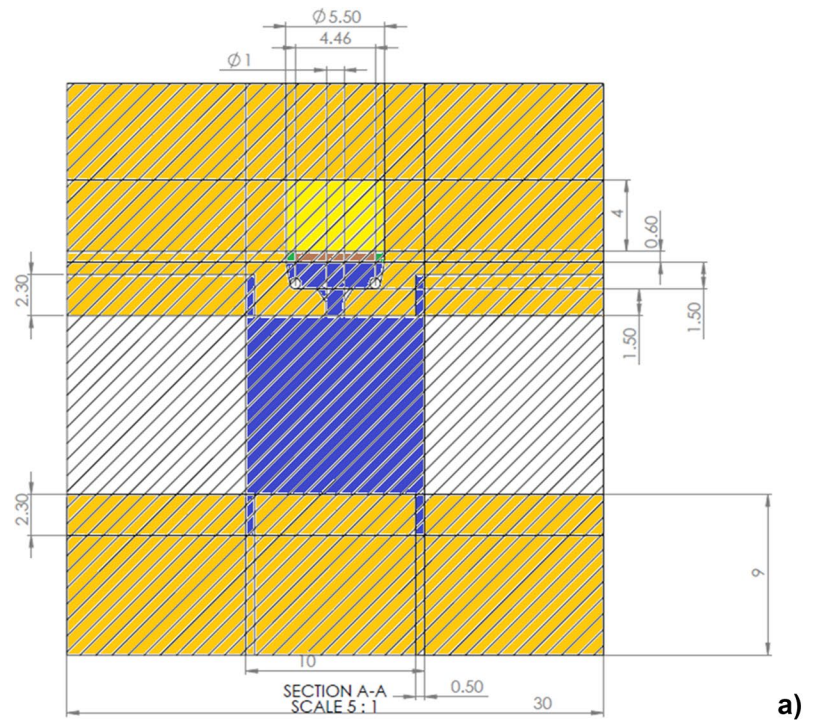


**Fig. 15** Example of particle accumulation structures formed as a result of the application of vibrations to the non-isothermal fluid (simulations conducted using ANSYS Fluent for a representative case, namely, standard heavy particles, vibrational mode 8 and  $\Delta T = 15$  K)

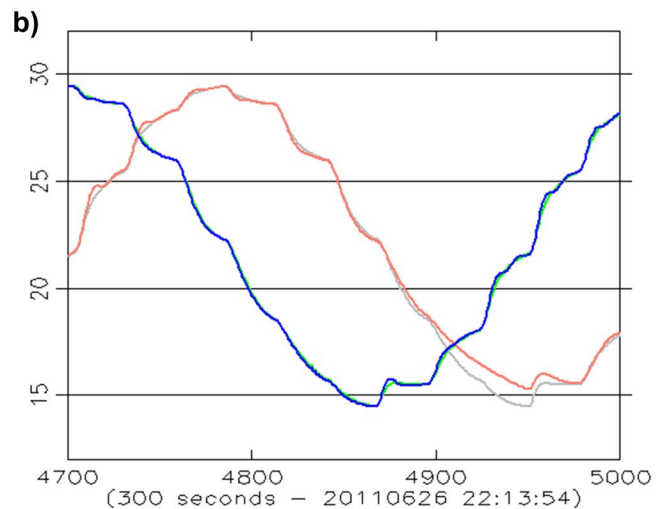
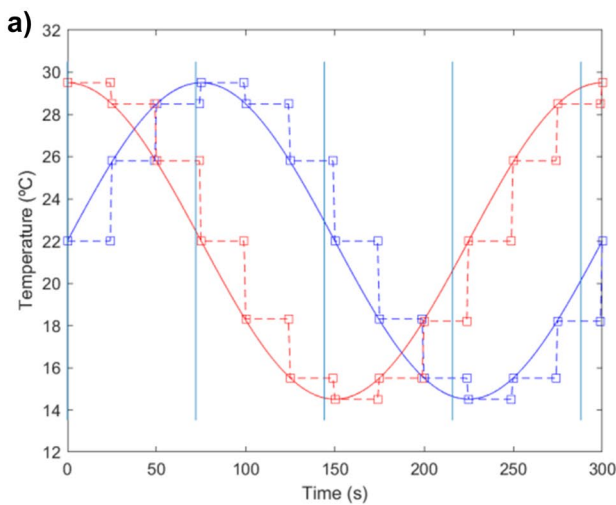
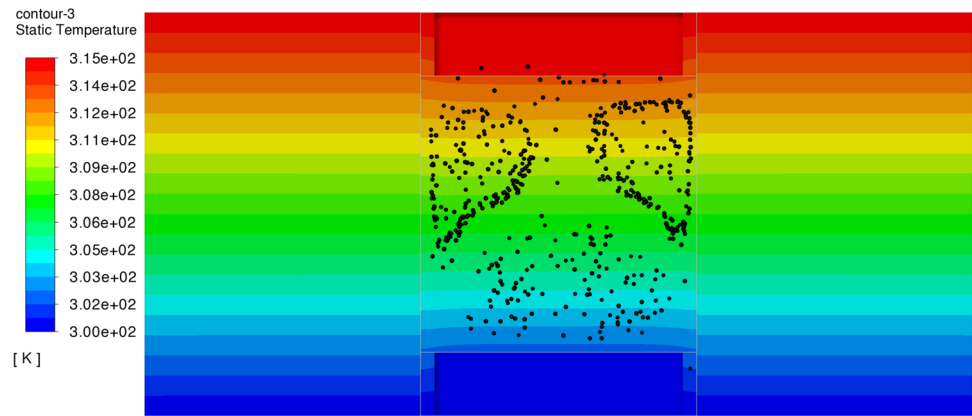


**Fig. 16** Temperature on the sidewalls during the modulation stage (Step 3): (a) theoretical temperature profile (courtesy of E-USOC), (b) measured temperature profile

where  $\Delta T_{mod} = 15$  °C and  $\omega_{therm}$  is the angular frequency of the thermal modulation. In this step a vibrational mode with relatively high acceleration amplitude is used to force particles to quickly leave the structures formed during step 3 (Fig. 17).

– **Step 5:** Shaking with thermal modulation is applied again with different (smaller) frequency and amplitude of vibrations to obtain a more uniform dispersion of particles in the liquid.

**Fig. 17** Example of particle distribution obtained after the combined application of vibrations and thermal modulation to the pre-existing particle structure shown in Fig. 15 (simulations conducted using ANSYS Fluent for standard heavy particles, vibrational mode 12 and period of thermal modulation 300 s)

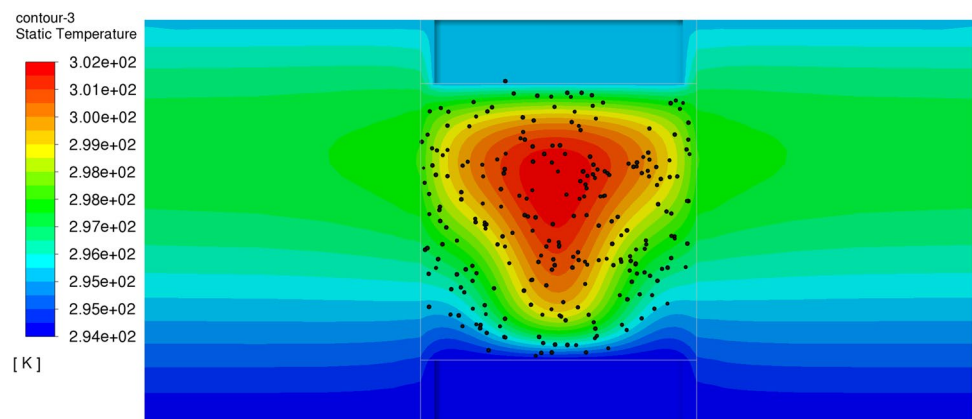


**Table 7** Parameter ranges considered for PARTICLE VIBRATION

Parameter	Range	Parameter	Range
$f$	1 – 2.8 (Hz)	$\Omega$	8380–23,300
$g_\omega$	2.8 – 9.6 (m/s <sup>2</sup> )	$\gamma$	$4.92 \times 10^8$ — $1.72 \times 10^9$
$\Delta T$	0.5 – 15 (°C)	$Ra_\omega$	$3 \times 10^4$ — $1.8 \times 10^6$
$\omega_{\text{therm}}$	$2.09 \times 10^{-2}$ — $4.18 \times 10^{-2}$ (rad/s)		

- **Stop and start:** After step 5, the shaker is switched off and a new run with new parameters ( $\Delta T$ ,  $b$ ,  $\omega$ ) can start (step 1).

After the completion of the last step, the vibration system is switched off and the system is ready for the execution of a new run (in general, no crew intervention is required). The experiment run (ER) is repeated at a different frequency and amplitude of vibration in both (primary and companion) cells.

It should be noted that from a practical point of view, thermal modulation envisaged in Steps 4 and 5 (see again Eqs. (6) and (7)) is implemented in the SODI scripts as a combination of step functions (the classical “sine” function is approximated using a staircase-shape sine waveform obtained with a sequence of *setpoint* and *wait* commands, Fig. 16).

In order to meet the criteria set by ESA in terms of allowed frequencies and not to exceed the maximum temperature difference allowed by the SODI instrument ( $\Delta T = 15$  °C), the runs have been defined (and, accordingly, scripts have been built) considering the ranges reported in Table 7 for vibrations frequency, acceleration amplitude, temperature difference and frequency of the thermal modulation (the ranges of the corresponding non-dimensional parameters defined in [Experiment governing parameters](#) are also included). The effective combination of such parameters for each run has been defined on the basis of dedicated numerical simulations conducted using the software described in Lappa (2014a,

[b](#), 2016c, 2017, 2019a, b) and Lappa and Burel (2020) and ANSYS Fluent (the treatment of related details is beyond the scope of the present work; the examples shown in Figs. 15 and 17 have been reported solely to support reader’s understanding of the sequence of events enabled by the different steps in which each experiment run is articulated).

## On the Ground Activities Conducted in Preparation of the Flight Experiment

### Compatibility Tests

As the work fluid used in PARTICLE VIBRATION differs from those used in previous SODI experiments, a specific procedure has been defined and implemented to qualify the new cells to assure that there is no long-term incompatibility between the fluid, the particles and the materials from which the cells are constructed. This has required a long-term (> 6 month) test campaign, which for practical reasons (the extremely high cost of the new hardware) has been conducted using representative cells filled with the effective liquid and particles to be used for the flight experiment.

It is also worth noticing that, prior to this test, short-duration (1 month) testing was executed with relevant candidate materials to allow any incompatibility to be identified early and therefore mitigate the risk of failure in the long-term verification activity.

**Fig. 18** Cells filled with ethanol and different particles types used for the long-duration compatibility tests



All cells used in the long-term compatibility tests were cells related to the earlier DCMIX experiment (where the acronym DCMIX stands for “diffusion coefficients of ternary fluid mixtures”, Shevtsova et al. 2014a, b; Triller et al. 2018). These cells, consisting of C11000\_E-Cu-99% nickel plated copper, quartz and AISI 303 stainless steel (used for the washer and plugs), have been considered due to their similarity with those envisaged by the PARTICLE VIBRATION project. They have been used in conjunction with the new DuPont™ Kalrez 6375 elastomers (i.e. specific sealing rings and membrane), selected for the PARTICLE VIBRATION experiment due to their expected ability to cope with ethanol.

The tests with the materials indicated in Tables 3, 4 and 5 have shown no significant oxidation phenomena (see, Fig. 18).

## Vibration Tests

The ground activities have not been limited to materials compatibility verification. Given the delicate nature of some of the particles listed in Table 5 (Silver Coated Hollow Glass with density  $0.14 \text{ g/cm}^3$ ), additional investigations have been conducted to assess the risk of particle breakage during acceptance testing of the flight hardware and/or due to the spectrum of vibrations produced during launch. The SpaceX launcher, currently envisaged for the launch of the PARTICLE VIBRATION hardware, can generate a significant amount of vibrations and noise during ignition, lift-off and atmospheric flight. For these reasons, any payload launched with it can experience a range of axial and lateral accelerations (in particular, axial acceleration is induced by vehicle thrust and drag profiles; while lateral accelerations are primarily driven by wind gusts, engine gimbal maneuvers, first-stage engine shutdown and other short-duration events, (Falcon’s user guide 2020). For both these axial and lateral components, the maximum predicted sinusoidal vibration environments for the Space X Falcon launcher correspond to approximately 0.5–0.6 g over the range of frequencies from 5 to 100 Hz. In addition, the random vibration environment includes several contributions, as indicated in the following (Falcon’s user guide 2020):

### 1. Low Frequency (0–100 Hz)

- Excitations driven by global vehicle motion and modes.
- sine vibration envelope this region.

### 2. Mid Frequency (100 Hz – 600 Hz)

- Excitation due to aero acoustics.
- Acoustic excitation and aero buffet are primary drivers in this region.

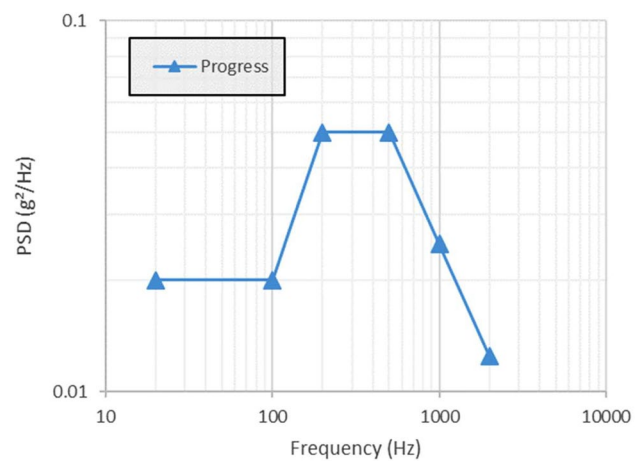


**Fig. 19** Power spectra density (PSD) as a function of frequency used for random vibration testing

### 3. High Frequency (600 Hz – 2000 Hz)

- Excitation due to structure borne vibration.
- Merlin Vacuum (MVac) forcing functions.

Accordingly, the following tests have been conducted to verify light particle response:

Sine sweep resonance research testing with acceleration level fixed to 0.5 g and vast frequency range (5–2000 Hz) and random vibration testing with power spectra density shown in Fig. 19 (this being conservative with respect to the conditions attained onboard the SpaceX).

This series of tests have yet been conducted using available representative hardware (namely, the IVIDIL ‘engineering model’ cell array containing two ethanol-filled cells, one with heavy and one with light particles). This cell array was packed in its stowage bag, as it would be before flight, and encapsulated into a rigid box (the ‘vibration jig’) as shown in Fig. 20a (the stowage bag was a snug fit in the rigid test container without any free space between it and the walls of the test container).

The verification has been conducted by applying random vibrations along all the axes of the reference system shown in Fig. 20b. One triaxial accelerometer (PCB type 356B21) has been fitted to the cell array. Due to limitations on the number of input channels available on the data acquisition system, only one response from one axis of this triaxial accelerometer has been used in any given test; the response in-line with the excitation axis. Moreover, vibration testing in the z-axis has been achieved by mounting the rigid container (with the PARTICLE VIBRATION cell array inside) directly on a vertical shaker by means of an interface clamp jig, as shown in Fig. 21a. For testing in the y- and x-directions, the rigid container was bolted to the shaker slip table via the same interface clamp jig, Fig. 21b.

**Fig. 20** Cell array in stowage bag (a), stowage bag packed in rigid container and sketch showing the reference axes (b)

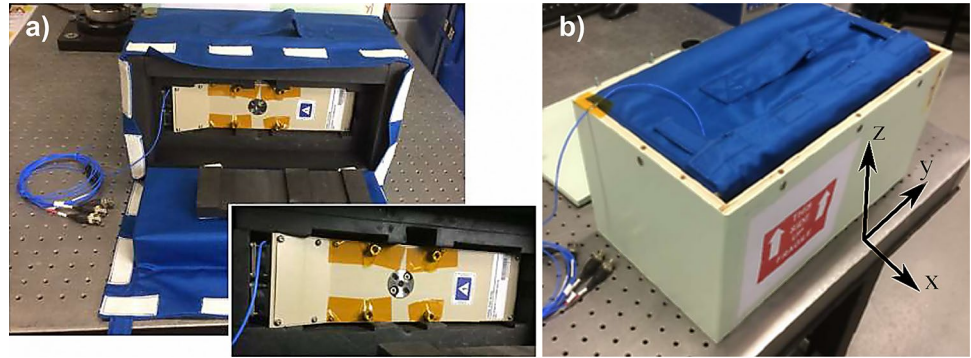
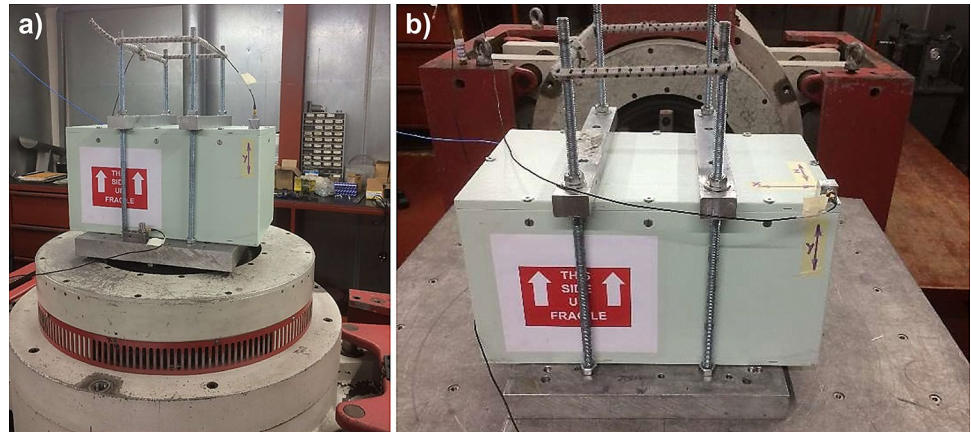


**Fig. 21** Cell array package on shaker for z-axis (a) and y- and x-axis (b) excitation



The final state of the particles has been assessed through comparative analysis of photographs of the cells before and after testing for each axis of vibration; moreover, since broken particle fragments sink, the amount of breakage has been quantitatively substantiated through visual inspection of the sedimented phase. Overall, launch vibrations have not been found to damage particles.

### Durability Testing of Tween 20

Additional dedicated testing has been implemented to verify the ability of the surfactant (the Tween 20 indicated in Table 4), needed to prevent particles from sticking to the walls of the cell during the flight experiments, to retain a stable chemical composition for temperatures slightly larger than those recommended by the manufacturer. The need for such additional level of verification has emerged from the ambient temperature limits for the aforementioned SpaceX launcher exceeding by 6 °C the stability threshold indicated by the company producing it (refer to [Materials \(Fluids and particles\)](#)).

Towards this end, small vials were prepared containing nickel and copper wires and particles submerged in ethanol with 0, 1, 2, and 4% of Tween 20 and left in a mechanical convection oven (BinderGmbH, Tuttlingen, Germany)

for two weeks at 46 °C, and inspected at regular intervals (Fig. 22). At the end of the experiment, no detrimental effect of the temperature on particle behavior has been identified. Vials of particles suspended in ethanol with 0%-4% (v/v) Tween 20 were also prepared at room temperature for long term durability tests. Due to some discoloration caused by a



**Fig. 22** Vials of the standard-heavy particles submerged in ethanol containing 0–4% Tween 20 after 2 weeks testing at 46 °C

reaction of the silver coating of the small-heavy and extra-heavy particles in 4% Tween 20, a concentration of 1% (v/v) Tween 20 has been judged as the most convenient one for the flight experiment.

The remainder of this paper is finally devoted to a presentation of the other ‘ad hoc’ procedures that have been designed and validated to achieve proper degassing of the involved liquid (to prevent it from forming undesired gas bubbles during experiment execution) and to fill the cells in terrestrial conditions (i.e. in the presence of gravity) with the required mixture of liquid and particles while fulfilling the following two objectives:

- ensuring that the unavoidable amount of particles broken (as a result of their interaction with the cell filling port and the tools used to displace them) remains within acceptable limits (compatible with the science objectives, i.e. no more than 20% of the total);
- ensuring that the total number of particles dispersed in the fluid matches the specific criteria set by the science team.

### Fluid Degassing

The degassing process for PARTICLE VIBRATION has been designed in order to encompass two distinct stages, namely: firstly, vapor degassing to remove as much of the trapped gasses as possible, and then the freeze–pump–thaw cycle to ensure complete gas removal. These steps are illustrated in detail in the following two subsections.

### Vapor Degassing

In this stage, approximately 50 ml of ethanol absolute is poured into a Duran bottle and sealed with a Vaplock cap with one port connected to the vacuum line and another connected to a vacuum gauge (Fig. 23a). A cold trap with liquid nitrogen is connected along the vacuum line to condense the vapor and prevent it from entering the pump. The ethanol is stirred on a magnetic hot plate at 30 °C to allow bubbles to rise to the surface and a vacuum of 95 kPa is concurrently applied for 10 min. A good vacuum hold has to be demonstrated by switching off the connecting valve between the vacuum and apparatus and maintaining the gauge position.

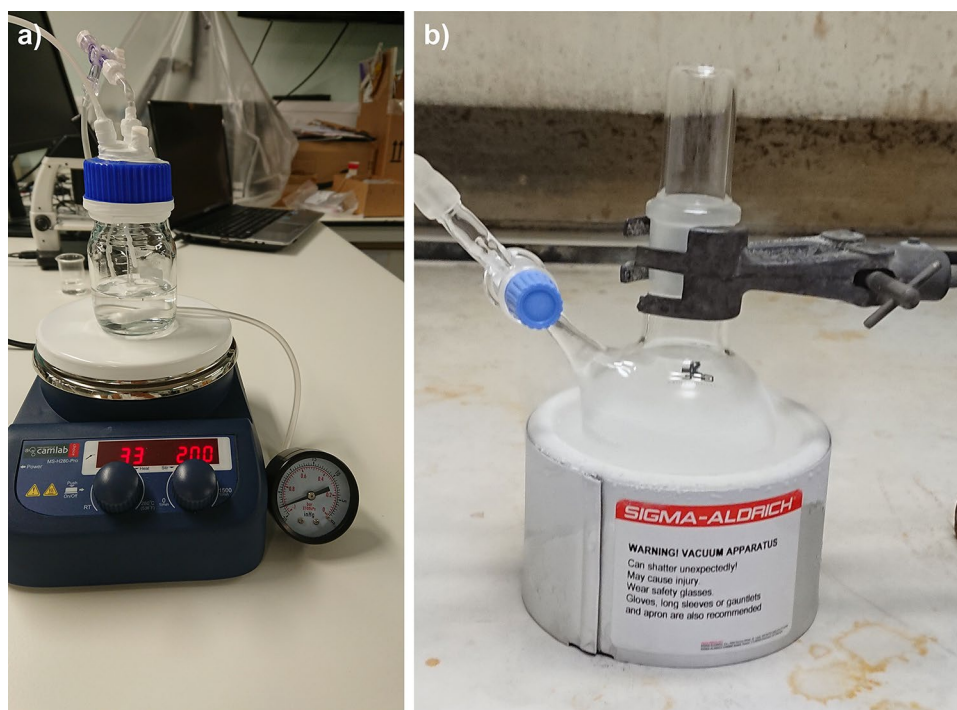
### Freeze–pump–thaw Process

To ensure complete degassing, the vapor degassed ethanol is then transferred (using a gas-tight syringe and keeping the syringe tip submerged to avoid recontamination) to a round bottom Schlenk flask where it undergoes a cyclic freeze–pump–thaw process under liquid nitrogen (Fig. 23b).

This involves 4 key steps:

1. Nitrogen gas is bubbled through the ethanol to displace any remaining oxygen and prevent liquid nitrogen from condensing the oxygen.
2. The Schlenk flask is submerged in a low form Dewar flask filled with liquid nitrogen in order to flash freeze the ethanol.

**Fig. 23** Fluid degassing activities: (a) the vapor degassing process and (b) the freeze–pump–thaw degassing process



3. Once the ethanol volume is fully frozen, the vacuum line is opened to remove all gases in the head space above the frozen liquid.
4. The ethanol is then allowed to thaw slowly, first at room temperature to prevent thermal shock, and then through the aid of a tepid water bath. The low pressure in the vacated head space enables trapped gases in the thawing ethanol to rise to the surface.

This process has to be repeated at least 3 times to ensure all gases are removed from the solvent (ethanol), which can be considered sufficient when no further bubbles rise to the vacated headspace. Immediately following degassing, the ethanol is slowly filled in SGE gastight syringes made of borosilicate glass equipped with a PTFE (Polytetrafluoroethylene) plunger and sealed with a stopcock, taking care to remove fluid from the base of the bottle to avoid any bubbles from entering. The syringes are tipped vertically to allow any residual bubbles to aggregate, which are then eliminated. To test if degassing is successful, a small bubble can be introduced in a degassed and control (non-degassed) syringe and left overnight. Disappearance of the bubble in the degassed syringe indicates that the fluid is below saturation (Fig. 24).

### Fluid Container Filling Procedure

Given the small size of the particles (see again Table 5) and their fragility in some cases (light particles made of hollow glass), determining their number precisely and preventing them from undergoing significant damage is not as straightforward as one would imagine. For this reason, several attempts have been made in order to optimize these processes.

The following provides a summary of the procedures which have proven successful in fulfilling these objectives.

### Particle Counting and Filling

500-5000  $\pm$  50 particles are taken from polypropylene centrifuge tubes using a micro spatula (Fig. 25a) and tipped carefully on to the end of a thin tool of aluminum or carbon ensuring a single layer formation of particles on the surface (Fig. 25b). An additional prior step is taken with the extremely fragile light particles prior to transferring them to the tool by suspending them in acetone. This serves two purposes, firstly to separate the broken particles (which will sink) from the sample and secondly, to remove any static charge present on the particles. The tool containing the particles is carefully transferred to a 5 M USB digital microscope (RS Components Ltd, Northants, UK) with  $\times$ 300 magnification for counting, using the manual counting tool in the “ImageJ” image processing software or through a more automated process using a macro. If there is an excess number of particles, the tool is gently tilted to release some particles and then recounted. Once counted, the tip of the tool is placed near the opening of the 1 mm port and tapped lightly to allow the particles to fall in, without necessitating any sweeping motion with rods or other tools, which could lead to breakages (Fig. 25c). A wide mouth aluminum micro-funnel with a 1 mm inner diameter tip is positioned over the filling port to facilitate this process. Since even through the aid of the funnel, some particles can remain on the innermost rim of the filling port (Fig. 25e), light tapping can be used to tip these particles into the cell (in general, as demonstrated by our tests, any remaining particles are sucked into the cell following application of vacuum). The

**Fig. 24** SGE gas tight syringes filled with degassed (top) and control (bottom) volume of ethanol with test bubble taken 24 h apart. Degassing considered successful following disappearance of the bubble (top right picture). +

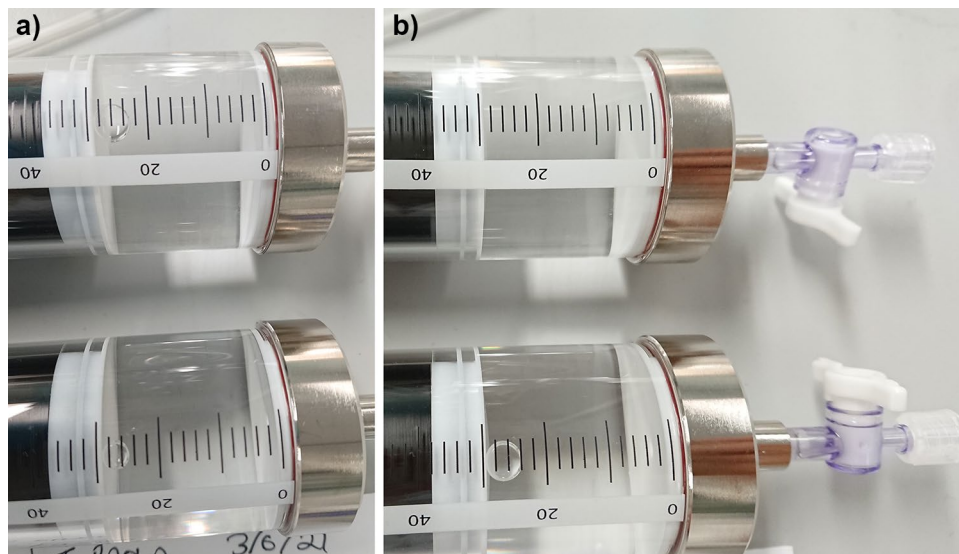
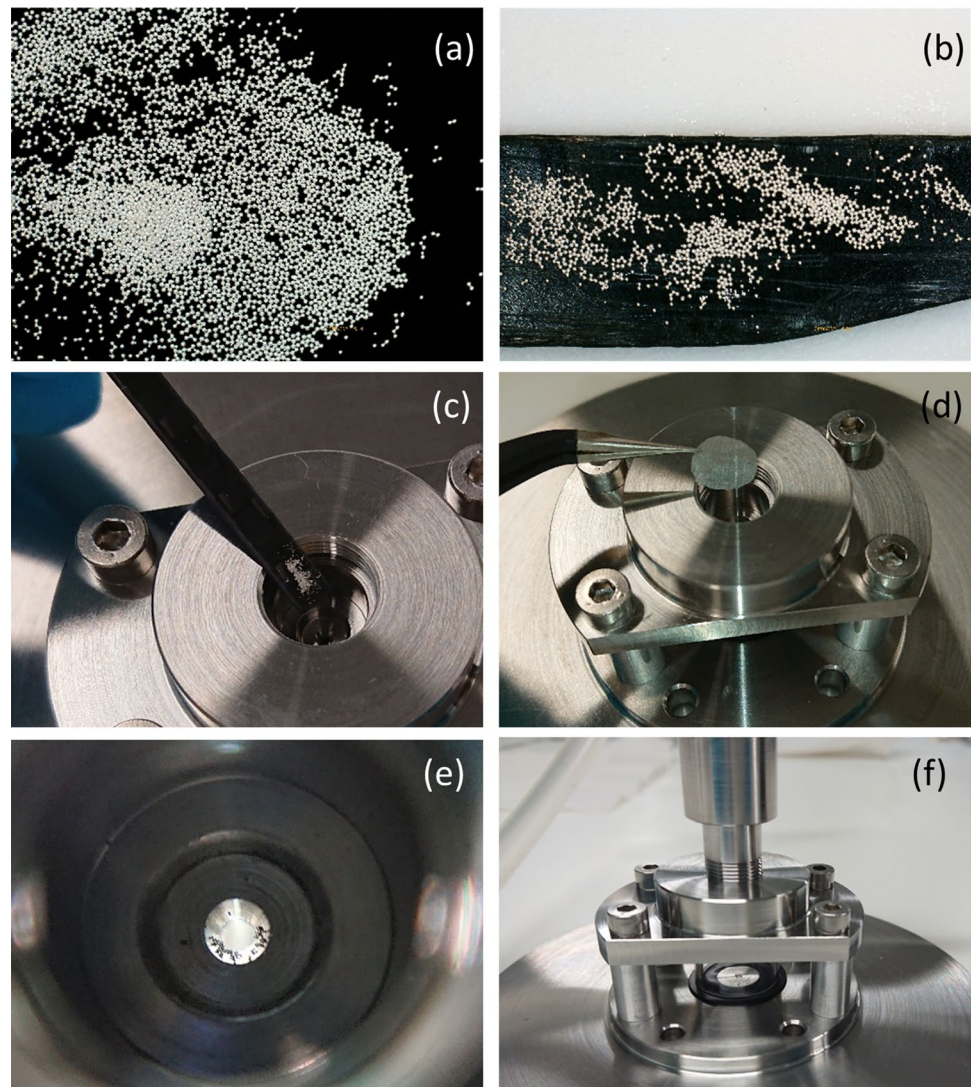


**Fig. 25** Cell filling procedure, (a) light particles under a 5 M USB digital microscope at  $\times 300$  magnification, (b) counted particles on carbon tool tip, (c) insertion of particles into the cell port, (d) application of a 25  $\mu\text{m}$  mesh, (e) some particles seated along the inner rim of filling port, and (f) application of the filling adaptor



tool is then returned to the microscope to count any remaining particles, which have to be deducted from the final count.

### Cell Filling Procedure

The main (five) steps of the procedure can be summarized as follows:

- 1) 1% (v/v) of Tween 20 (see again Table 4 for the related details) is added to the cell using a glass syringe mounted with a fine needle. Given the oxidative and hydrolytic nature of the surfactant (see Donbrow et al. 1978), care must be taken to ensure it remains unexposed to bright light or high temperatures prior to the start of the experiments.
- 2) A 25  $\mu\text{m}$  steel mesh is inserted over the filling port to prevent particles escaping following application of the vacuum and a filling adaptor is connected to the threaded joint of the cell (Fig. 25d).
- 3) The filling adaptor and T-piece (Fig. 25f and

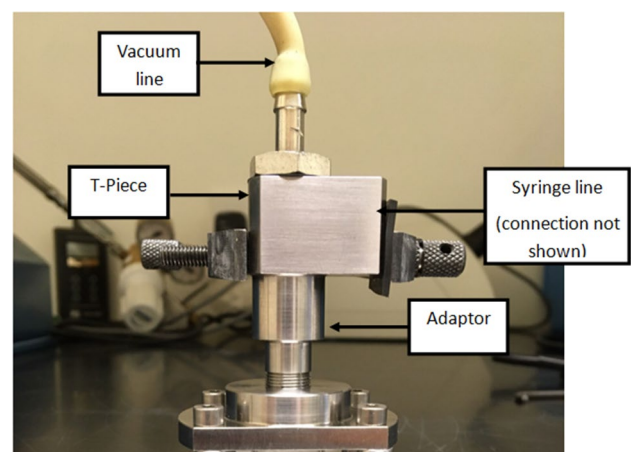


**Fig. 26** Filling adaptor and T-piece connected to the cell with vacuum applied through the top intake of the T-piece

Fig. 26) are connected to the cell and a vacuum is applied through the top intake of the T-piece and maintained. 4) Once a deep vacuum is reached (considered at > 95 kPa), a valve connecting a glass syringe filled with the degassed ethanol to the T-piece is opened to allow slow filling of the cell with the solvent. Ensuring any bubble is removed through use of the syringe, the adaptor and T-piece are then removed, and the cell ‘topped up’ with degassed ethanol to the rim of the top plug. 5) The mesh is then removed and replaced with the compensation system and the cell is finally sealed tight with a washer and plug. A final visual inspection is carried out to ensure particles have been properly seeded and no residual bubbles are present in the cell.

## Conclusions

In this paper, we have presented the PARTICLE-VIBRATION project giving emphasis to the instrument, the scientific protocols and the related ‘functional interrelations’. These new experiments have been conceived to take full advantage of the Selectable Optical Diagnostic Instrument (SODI) and the Microgravity Science Glovebox (MSG). These payloads allow ‘remote’ (from the ground) control of the experiment thereby leading to notable savings in terms of hardware cost and crew time.

The materials, parts, sub-systems and new hardware manufactured on purpose, have been designed to allow meaningful exploration of the vast space of parameters underpinning the considered category of phenomena. The temperature difference applied across the fluid samples can be varied while the amplitude and frequency of the applied vibrations can be controlled independently, thereby resulting in a variety of fluid-dynamic regimes where particles can self-assemble and produce highly ordered accumulation structures with varying sizes, morphology and formation times. These can be observed using the optical modules of this facility, by which high-resolution images can be taken with a desired frequency and saved on board the ISS on a dedicated disk (and directly transferred to ground for nearly real-time assessment).

Implementing the PARTICLE VIBRATION project has required proper testing of materials compatibility (for the cell arrays) and refurbishment of the sub-system used to generate the vibrations (the shaker). Moreover additional on-the-ground activities have been designed and optimized to ensure proper degassing of the considered fluid-particle mixtures and avoid damage of particles (especially the light ones) during on-the-ground preparatory work (i.e. filling of the flight cells and/or due to exposure to the spectrum of accelerations produced during the launch). The present work naturally complements a set of earlier studies where such technological aspects were overlooked, or glossed over in

favor of purely scientific details, thereby providing (together with those works) a complete picture of the PARTICLE VIBRATION project.

**Acknowledgements** This work has been supported by the UK Space Agency (STFC grants ST/S006354/1, ST/V005588/1, ST/W002256/1 and ST/W007185/1) in the framework of the PARTICLE VIBRATION (T-PAOLA) project.

**Funding** Science and Technology Facilities Council, ST/S006354/1, Marcello Lappa, ST/V005588/1, Marcello Lappa, ST/W002256/1, Marcello Lappa, ST/W007185/1, Marcello Lappa.

## Declarations

**Conflict of Interest** The authors declare that they have no conflict of interest.

**Open Access** This article is licensed under a Creative Commons Attribution 4.0 International License, which permits use, sharing, adaptation, distribution and reproduction in any medium or format, as long as you give appropriate credit to the original author(s) and the source, provide a link to the Creative Commons licence, and indicate if changes were made. The images or other third party material in this article are included in the article's Creative Commons licence, unless indicated otherwise in a credit line to the material. If material is not included in the article's Creative Commons licence and your intended use is not permitted by statutory regulation or exceeds the permitted use, you will need to obtain permission directly from the copyright holder. To view a copy of this licence, visit <http://creativecommons.org/licenses/by/4.0/>.

## References

- Albanese, C., Carotenuto, L., Ceriello, A., Dell’Aversana, P., Fortezza, R., Lappa, M., Peluso, F., Pezzuti, F., Piccolo, C., Tempesta, S., Verzino, G., Bonnat, G., Pensavalle, E., Marangoni, R., Rina, L., Trincherò, G.: “Fluid Science Laboratory: Ready to fly! Lessons learned on preparatory activities, operations and performances”, 58th Congress of the International Astronautical Federation, 2007, 24–28 September 2007, Hyderabad, India, paper number: IAC-07-A2.5.02, **1**, 2007, Pages 564–570 (2007) (ISBN: 978–160560150–2). <https://www.iafastro.net/iac/archive/browse/IAC-07/A2/5/7855/>
- Albanese, C., Ceriello, A., Castagnolo, D., di Costanzo, G., Lappa, M., Piccolo, C., Sorrentino, D., Tempesta, S.: “A complex operational scenario for the execution of European fluid physics experiments on the ISS: achievements and lessons learned”, 61st Int. Astronaut. Cong. (Prague, Czech Republic, 27/9/10–01/10/2010), paper number: IAC-10.A2.7.3, Volume **12**, 2010, Pages 10288–10295 (ISBN: 978–161782368–8) (2010). <https://www.iafastro.net/iac/archive/browse/IAC-10/A2/7/9140/>
- Boaro, A., Lappa, M.: Multicellular States of Viscoelastic Thermovibrational Convection in a Square Cavity. *Phys. Fluid.* **33**(3), 033105 (18 pages) (2021a)
- Boaro, A., Lappa, M.: On the competition of overstability and stabilizing effects in viscoelastic Thermovibrational flow. *Phys. Rev. E.* **104** (2), 025102 (17 pages) (2021b)
- Born, P., Braibanti, M., Cristofolini, L., Cohen-Addad, S., Durian, D.J., Egelhaaf, S.U., Escobedo-Sánchez, M.A., Höhler, R., Karapantsios, T.D., Langevin, D., Liggieri, L., Pasquet, M.,

- Rio, E., Salonen, A., Schröter, M., Sper, M., Sütterlin, R., Zuccolotto-Bernez, A.B.: Soft matter dynamics: A versatile microgravity platform to study dynamics in soft matter, *Rev. Sci. Instrum.* **92**, 124503 (15 pages) (2021)
- Capobianchi, P., Lappa M.: Particle accumulation structures in non-cylindrical liquid bridges under microgravity conditions. *Phys. Rev. Fluid.* **5**(8), 084304 (30 pages) (2020)
- Capobianchi, P., Lappa, M.: Particle accumulation structures in a 5 cSt silicone oil liquid bridge: New data for the preparation of the JEREMI Experiment, *Micrograv. Sci. Tech.* **33**,31 (12 pages) (2021b)
- Capobianchi, P., Lappa, M.: On the influence of gravity on particle accumulation structures in high aspect-ratio liquid bridges. *J. Fluid. Mech.* **908**, 10 February 2021b, A29 (30 pages) (2021a)
- Carotenuto, L., Piccolo, C., Castagnolo, D., Lappa, M., Garcia-Ruiz, J.M.: Experimental observations and numerical modelling of diffusion-driven crystallisation processes. *Acta Crystallographica D* **58**, 1628–1632 (2002)
- Crewdson, G., Lappa, M.: Thermally-driven flows and Turbulence in Vibrated liquids. *Int. J. Thermofluids.* **11**, 100102 (20 pages) (2021a)
- Crewdson, G., Lappa, M.: The zoo of modes of convection in liquids vibrated along the direction of the temperature gradient, *FLUIDS*, **6**(1), 30 (23 pages) (2021b)
- Deng, X., Chawla, N.: Modeling the effect of particle clustering on the mechanical behaviour of SiC particle reinforced Al matrix composites. *J. Mater. Sci.* **41**(17), 5731–5734 (2006)
- Dhir, V.K., Warriar, G.R., Aktinol, E., et al.: Nucleate Pool Boiling Experiments (NPBX) on the International Space Station. *Microgravity Sci. Technol.* **24**, 307–325 (2012). <https://doi.org/10.1007/s12217-012-9315-8>
- Donbrow, M., Azaz, E., Pillersdorf, A.: Autoxidation of Polysorbates. *J. Pharm. Sci.* **67**(12), 1676–1681 (1978)
- Dubert, D., Marín-Genescà, M., Simón, M.J., Ezquerro, J.M., Massons, J., Jna, G., Ruiz, X., Shevtsova, V.: On the Monitoring of the Vibratory Environment of DCMIX4 Campaign. Preliminary Results. *Microgravity Sci. Technol.* **32**, 615–628 (2020)
- Futterer, B., Dahley, N., Koch, S., Scurtu, N., Egbers, C.: From isoviscous convective experiment ‘GeoFlow I’ to temperature-dependent viscosity in ‘GeoFlow II’—Fluid physics experiments on-board ISS for the capture of convection phenomena in Earth’s outer core and mantle. *Acta Astronaut.* **71**, 11–19 (2012)
- Hashimoto, H., Fukatsu, T., Ano, Y., Mizuno, M., Hashimoto, T., and Tokumura T.: “Development of international standard payload rack structure for space station science operations”, 36th AIAA Aerospace Sciences Meeting and Exhibit, 12 January 1998 - 15 January 1998, Reno, NV,U.S.A. (1998).<https://doi.org/10.2514/6.1998-466>
- Irace, P.H., Lee, H.J., Waddell, H., Tan, L., Stocker, D.P., Sunderland, P.B., Axelbaum, R.L.: Observations of long duration microgravity spherical diffusion flames aboard the International Space Station. *Combust. Flame.* **229**, 111373 (2021)
- Kawamura, H., Ueno, I., Ishikawa, T.: Study of thermocapillary flow in a liquid bridge towards an on-orbit experiment aboard the international space station, *Adv. Space. Res.* **29**(4), 611–618 (2002). <https://www.sciencedirect.com/science/article/abs/pii/S0273117701006512>
- Kitmacher, G.: 2010. Create Space Independent Publishing Platform, Reference Guide to the International Space Station (2010)
- Kuhlmann, H.C., Lappa, M., Melnikov, D., Mukin, R., Muldoon, F.H., Pushkin, D., Shevtsova, V.S., Ueno, I.: The JEREMI-Project on thermocapillary convection in liquid bridges. Part A: Overview of Particle Accumulation Structures. *Fluid Dyn. Mater. Process.* **10** (1), 1–36 (2014)
- Lappa, M., Boaro, A.: Viscoelastic Thermovibrational Flow Driven by Sinusoidal and Pulse (Square) Waves, *FLUIDS*. **6**(9):311 (15 pages) (2021)
- Lappa, M., Burel, T.: Symmetry Breaking Phenomena in Thermovibrationally Driven Particle Accumulation Structures. *Phys. Fluids.* **32**(5):053314 (23 pages) (2020)
- Lappa, M.: *Fluids Materials and Microgravity: Numerical techniques and insights into the physics*, Elsevier Science (2004. England), Oxford (2004)
- Lappa, M.: Assessment of VOF Strategies for the analysis of Marangoni Migration. Collisional Coagulation of Droplets and Thermal Wake Effects in Metal Alloys under Microgravity Conditions, *Computers, Materials & Continua CMC* **2**(1), 51–64 (2005)
- Lappa, M.: A theoretical and numerical multiscale framework for the analysis of pattern formation in protein crystal engineering. *Int. J. Multiscale Comp. Eng.* **9**(2), 149–174 (2011)
- Lappa, M.: “Assessment of the role of axial vorticity in the formation of Particle Accumulation Structures (PAS) in supercritical Marangoni and hybrid thermocapillary-rotation-driven flows”. *Phys. Fluids.* **25**(1):012101 (11 pages) (2013a)
- Lappa, M.: On the variety of particle accumulation structures under the effect of g-jitters. *J. Fluid Mech.* **726**, 160–195 (2013b)
- Lappa, M.: The patterning behaviour and accumulation of spherical particles in a vibrated non-isothermal liquid. *Phys. Fluids.* **26**(9), 093301 (2014a)
- Lappa, M.: On the nature, formation and diversity of particulate coherent structures in Microgravity Conditions and their relevance to materials science and problems of Astrophysical interest. *Geophys. Astrophys. Fluid Dyn.* **110**(4), 348–386 (2016a)
- Lappa, M.: Control of convection patterning and intensity in shallow cavities by harmonic vibrations. *Microgravity Sci. Technol.* **28**(1), 29–39 (2016b)
- Lappa, M.: Numerical study into the morphology and formation mechanisms of three-dimensional particle structures in vibrated cylindrical cavities with various heating conditions, *Phys. Rev. Fluid.* **1**(6), 064203 (2016c)
- Lappa, M.: On the multiplicity and symmetry of particle attractors in confined non-isothermal fluids subjected to inclined vibrations. *Int. J. Multiphase Flow* **93**, 71–83 (2017)
- Lappa, M.: On the formation and morphology of coherent particulate structures in non-isothermal enclosures subjected to rotating g-jitters, *Phys. Fluids.* **31**(7), 073303 (11 pages) (2019a)
- Lappa M.: Time reversibility and non-deterministic behaviour in oscillatorily sheared suspensions of non-interacting particles at high Reynolds numbers. *Comput. Fluids* **184**, 78–90 (2019b)
- Lappa, M., Piccolo, C., Esposito, G., Giordano, D., La Gala, S., Sorrentino, D., De Chiara, G., Di Costanzo, G., Fortezza, R., Albanese, C.: “The SODI Diffusion Soret Coefficient Experiment onboard ISS: a flexible and modular approach to operations in orbit”, 63rd International Astronautical Congress 2012 (Naples, Italy, 1–5 October 2012), paper number: IAC-12.A2.5.9x15283, **2**, 2012, Pages 892–899 (ISBN: 978–162276979–7) (2012). <http://www.iafastro.net/iac/archive/browse/IAC-12/A2/5/15283/>
- Lappa, M.: Stationary Solid Particle Attractors in Standing Waves. *Phys. Fluid.* **26**(1), 013305 (12 pages) (2014b)
- Lee, H.M., Park, O.O.: Rheology and dynamics of immiscible polymer blends. *J. Rheol.* **38**, 1405–1425 (1994)
- Mason, G.: New fundamental concepts in emulsion rheology. *Curr. Opin. Colloid Interface Sci.* **4**, 231–238 (1999)
- Mazzoni, S., Potenza, M.A.C., Alaimo, M.D., Veen, S.J., Dielissen, M., Leussink, E., Dewandel, J.-L., Minster, O., Kufner, E., Wegdam, G., Schall, P.: SODI-COLLOID: A combination of static and dynamic light scattering on board the International Space Station. *Rev. Sci. Instrum.* **84**, 043704 (2013). <https://doi.org/10.1063/1.4801852>
- Mialdun, A., Minetti, C., Gaponenko, Y., Shevtsova, V., Dubois, F.: Analysis of the Thermal Performance of SODI Instrument for DCMIX Configuration. *Microgravity Sci. Technol.* **25**, 83–94 (2013)

- Mialdun, A., Ryzhkov, I., Khlybov, O., Lyubimova, T., Shevtsova, V.: Measurement of Soret coefficients in a ternary mixture of toluene-methanol-cyclohexane in convection-free environment. *J. Chem. Phys.* **148**, 044506 (2018)
- Mialdun, A., Bou-Ali, M.M., Braibanti, M., Croccolo, F., Errarte, A., Ezquerro, J.M., Fernández, J.J., García-Fernández, L., Galand, Q., Gaponenko, Y., Gavalda, F., Köhler, W., Lyubimova, T., Ortiz de Zárate, J.M., Rodríguez, J., Ruiz, X., Ryzhkov, I.I., Schraml, M., Shevtsova, V., Van Vaerenbergh, S., Yasnou, V., Bataller, H.: Data quality assessment of Diffusion Coefficient Measurements in ternary mixtures 4 (DCMIX4) experiment. *Acta Astronaut.* **176**, 204–215 (2020)
- Mirihanage, W.U., Browne, D.J., Zimmermann, G., Sturz, L.: Simulation of international space station microgravity directional solidification experiments on columnar-to-equiaxed transition. *Acta Mater.* **60**(18), 6362–6371 (2012)
- Perminov, A.V., Lyubimova, T.P., Nikulina, S.A.: Influence of High Frequency Vertical Vibrations on Convective Regimes in a Closed Cavity at Normal and Low Gravity Conditions. *Microgra. Sci. Tech.* **33**, 55 (2021)
- Prinz, B., Romero, A.: New Casting Process for Hypermonotectic Alloys, in Immiscible liquid metals and organics, Proceedings of an international workshop organized by the ESA expert working group, "Immiscible alloys" held in the Physikzentrum, Bad Honnef 1992, edited by L. Ratke 1993, Germany, 281–289 (1993)
- Pushkin, D.O., Melnikov, D.E., Shevtova, V. M.: Ordering of small particles in one-dimensional coherent structures by time-periodic flows, *Phys. Rev. Lett.* **106**, 234501 (2011)
- Ratke, L.: "Decomposition, Phase separation, Solidification of immiscible liquid alloys", in Immiscible liquid metals and organics, Proceedings of an international workshop organized by the ESA expert working group, "Immiscible alloys" held in the Physikzentrum, Bad Honnef 1992, edited by L. Ratke, (Informationsgesellschaft, Verlag, Germany, 3–34 (1992)
- Roths, T., Friedrich, C., Marth, M., Honerkamp, J.: Dynamics and rheology of the morphology of immiscible polymer blends - on modeling and simulation. *J. Rheologica. Acta.* **41**(3), 211–222 (2002)
- Schraml, M., Triller, T., Sommermann, D., Köhler, W.: The DCMIX project: Measurement of thermodiffusion processes in ternary mixtures on ground and in space. *Acta Astronaut.* **160**, 251–257 (2019)
- Schwabe, D., Hintz, P., Frank, S.: New features of thermocapillary convection in floating zones revealed by tracer particle accumulation structures (PAS), *Microgravity Sci. Technol.* **9**, 163–168 (1996)
- Shevtsova, V., Gaponenko, Y., Kuhlmann, H.C., Lappa, M., Lukasser, M., Matsumoto, S., Mialdun, A., Montanero, J.M., Nishino, K., Ueno, I.: The JEREMI-Project on Thermocapillary Convection in Liquid Bridges. Part B: Impact of Co-Axial Gas Flow, *Fluid Dynamics & Materials Processing* **10**(2), 197–240 (2014a)
- Shevtsova, V., Kuhlmann, H., Montanero, J.M., Nepomnyaschy, A., Lappa, M., Schwabe, D., Matsumoto, S., Nishino, K., Ueno, I., Yoda S.: "Preparation of Space experiment in the FPEF facility: Heat transfer at the interface in the systems with cylindrical symmetry", 26th International Symposium on Space Technology and Science. Hamamatsu City (ISTS Proceedings) 1–8 (2008). [http://archive.ists.or.jp/upload\\_pdf/2008-h-03.pdf](http://archive.ists.or.jp/upload_pdf/2008-h-03.pdf)
- Shevtsova, V., Lyubimova, T., Saghir, Z., Melnikov, D., Gaponenko, Y., Sechenyh, V., Legros, J.C., Mialdun A.: "IVIDIL: On-board g-jitters and diffusion controlled phenomena," *J. Phys. Conf. Ser.* **327**, 012031 (2011a)
- Shevtsova, V., Mialdun, A., Melnikov, D., Ryzhkov, I., Gaponenko, Y., Saghir, Z., Lyubimova, T., Legros, J.C.: The IVIDIL experiment onboard the ISS: Thermodiffusion in the presence of controlled vibrations. *Compt. Rend. Mécaniq.* **339**(5), 310–317 (2011b)
- Shevtsova, V., Santos, C., Sechenyh, V. et al.: Diffusion and Soret in Ternary Mixtures. Preparation of the DCMIX2 Experiment on the ISS. *Microgra. Sci. Technol.* **25**, 275–283 (2014b)
- Sommermann, D., Triller, T., Köhler, W.: A Robust Data Evaluation Method for the DCMIX Microgravity Experiments. *Microgravity Sci. Technol.* **31**, 465–474 (2019)
- Space, X.; FALCON USER'S GUIDE, April 2020, Space Exploration Technologies Corp. (2020). [https://www.spacex.com/media/falcon\\_users\\_guide\\_042020.pdf](https://www.spacex.com/media/falcon_users_guide_042020.pdf)
- Triller, T., Bataller, H., Bou-Ali, M.M., Braibanti, M., Croccolo, F., Ezquerro, J.M., Galand, Q., Jna, G., Lapeira, E., Laverón-Simavilla, A., Lyubimova, T., Mialdun, A., Ortiz de Zárate, J.M., Rodríguez, J., Ruiz, X., Ryzhkov, I.I., Shevtsova, V., Van Vaerenbergh, S., Köhler, W.: Thermodiffusion in Ternary Mixtures of Water/Ethanol/Triethylene Glycol: First Report on the DCMIX3-Experiments Performed on the International Space Station. *Microgravity Sci. Technol.* **30**(3), 295–308 (2018)
- Trincherro, G., Cardano, M., Pensavalle, E., Bassano, E., Dell'Aversana, P., Lappa, M., Tacconi, M.: "The Fluid Science Laboratory on the ISS Columbus module Performances and Operations", *JASMA: J. Japan Soc. Micro. Appl.* (ISSN: 0915–3616) **25**(3): 303–308 (2008)
- Utracki, L.A.: Melt flow of polymer blends. *Polym. Eng. Sci.* **23**(11), 602–609 (1983)
- Zaussinger F., Haun P., Szabo P.S.B., Travnikov V., Al Kawwas M., Egbers C.: Rotating spherical gap convection in the GeoFlow International Space Station (ISS) experiment. *Phys. Rev. Fluids.* **5**, 063502 (2020)

**Publisher's Note** Springer Nature remains neutral with regard to jurisdictional claims in published maps and institutional affiliations.